UNIVERSITY OF LATVIA
MEDICAL FACULTY

COMPARISON OF DIFFERENT TECHNIQUES FOR THE QUANTITATIVE MEASUREMENT OF THE MOTILITY OF THE NASAL VALVE

MEDICAL DOCTOR DEGREE
DIPLOMA THESIS

Author

Lucas van Boemmel

lv13106

Supervisors

Prof. Dr. Dr. Klaus Vogt

Kaspars Peksis MD

Rīga 2019

Table of Contents

Abstract

Introduction

4-phase rhinomanometry is at present the only nasal airway function test that takes the elastic structures of the nasal airway into consideration. Following the recent discovery that nasal valve motility sets in early in nasal breathing, it is of fundamental value to establish a viable diagnostic instrument for the nasal valve as an elastic structure of the nasal airway.

Aim

The aim of this pilot study is to further the research of diagnostics of the pathological and physiological variations of the nasal airstream. The objective is to develop and advance initial measurement techniques that contribute to the implementation of a medical device for nasal valve elastography.

Materials and Methods

Various types of sensors were selected and tested, including inductive, optical, strain gauge sensors and a nano-camera. They were first built into clinically applicable devices, then tested in a laboratory setting and, if viable, brought into the participant-testing stage. 10 healthy participants were selected. They underwent preemptive 4-phase rhinomanometry to evaluate nasal function present prior to the assessment of sensor measurements.

Results

Obtaining quantitative data of the motility of the nasal valve was possible. The range of nasal valve motility during calm breathing may be as low as ± 0.5 mm. Video-based diagnostics have yet to be improved and give at present only subjective information. Inductive sensing and low-grade optical sensors seem unsuitable for the clinical setting. The high-grade optical sensors proved to be essential measuring and reference instruments. The strain gauge measurement technique is, in theory, a precise and practical method that needs further refinement and development into a medical product.

Conclusion

In surgical interventions directed at or inclusive of the nasal valve, its dynamic physiology should be considered. Elastographic measurement techniques should be developed to support the existing 4-phase rhinomanometry and computational fluid dynamics in nasal function diagnostics.

Diplomdarba kopsavilkums

Ievads

4-fāžu rinomanometrija šobrīd ir vienīgā nazālo elpceļu funkcionalitātes mērīšanas metode, kura ņem vērā nazālo elpceļu elastīgās struktūras. Sekojot līdz jaunākajiem atklājumiem par to kā nazālās vārstules kustīgums iedarbojas jau agri elpošanas ciklā, fundamentāli ir izveidot ilgtspējīgu diagnostikas instrumentu, kas mēra nazālo elpceļu elastīgās struktūras, it īpaši deguna vārstules.

Mērķis

Šī pilotpētījuma mērķis ir virzīt uz priekšu zinātnisko pētniecību fizioloģiskas un patoloģiskas deguna gaisa plūsmas diagnostikā. Mērķis ir attīstīt provizoriskas mērīšanas tehnikas, kas veicinātu nazālās vārstules elastogrāfijas ierīces ieviešanu medicīnā.

Materiāli un metodes

Tika testēti dažādi sensoru tipi, ieskaitot induktīvus, optiskus, deformācijas mērošus sensorus un nanokameras. Vispirms tie tika iekonstruēti klīnikā pielietojamās ierīcēs, tad testēti laboratorijas vidē. Ja tie bija ilgtspējīgi, tie tika pārnesti uz nākamo posmu ar brīvprātīgo testēšanu. Tika izvēlēti 10 veseli dalībnieki. Dalībniekus preemtīvi novērtēja ar 4-fāžu rinomanometriju, lai uzzinātu deguna funkcionalitāti pirms mērīšanas ar sensoriem.

Rezultāti

Izdevās iegūt kvantitatīvus datus par nazālo vārstuļu kustīgumu. Deguna vārstules kustīguma diapazons mierīgas elpošanas laikā var būt ± 0.5 mm šaurs. Būtu jāuzlabo videodiagnostika, jo šobrīd tā spēj sniegt tikai subjektīvu informāciju. Induktīvi sensori un zemas pakāpes optiskie sensori šķiet nepiemēroti klīniskai videi. Par būtiskiem mērīšanas un references instrumentiem izrādījās augstās klases optiskie sensori. Deformācijas mērīšanas tehnika teorētiski ir precīza un praktiska metode, kurai ir nepieciešama tālāka pilnveidošana un attīstība, lai kļūtu par produktu medicīnā.

Secinājumi

Nazālās vārstules dinamisko fizioloģiju vajadzētu ņemt vērā ķirurģiskajās procedūrās, kurās tiek iekļauta šī vārstule. Ir vajadzība attīstīt elastogrāfiskās mērīšanas tehnikas, lai komplektētu esošo 4-fāžu rinomanometriju un skaitļojošo modelēšanu deguna funkcionalitātes.

Introduction

The concept of this pilot study is to innovate and develop preliminary measurement techniques that can be advanced into medical products.

Consequently, our project follows into the footsteps of the strain gauge project by Akmenkalne (Akmenkalne et. al. 2018) in the quest of implementing a diagnostic tool to reliably measure the elasticity of the nasal valve. Thus, helping us to improve our understanding of the dynamic airway and establish its importance for nasal function diagnostics.

Vogt et al. drew attention to the value of 4-phase rhinomanometry in “Four-phase rhinomanometry: a multicentric retrospective analysis of 36,563 clinical measurements” in 2016 (Vogt et al. 2016) as the only currently viable method for nasal function testing that is inclusive of elastic structures such as the nasal valve.

Aim of the study

To innovate, advance and compare objective methods for the measurement of the nasal valve motility.

Objectives of the study

1. Development of measuring apparatuses fit to be used in clinical practice
2. Obtaining quantifiable measurements of the motility of the lateral nasal wall during nasal breathing
3. Comparison and verification of sensing modalities in their repeatability, practicability, accuracy and economic impact

Hypothesis

The nasal valve is in motion, even during calm nasal breathing. It is an essential part of the dynamic nasal airway and its physiological and pathological impact is likely of great significance for rhinological diagnostics and surgical interventions.

Literature Review

1.1 Anatomy and Physiology of the Nose

The anatomy of both the external and internal nose have a great impact on the performance of the nasal valve and, subsequently, play together in providing healthy nasal function.

1.1.1 Anatomy of the External and Internal Nose

Anatomy of the External Nose

The shape and structure of the external nose does not only influence the aesthetic appearance of the face but also takes part in the patency and functionality of the upper respiratory airway. Its elements take part in forming an active physiological gateway in respiration (Probst et al. 2018).

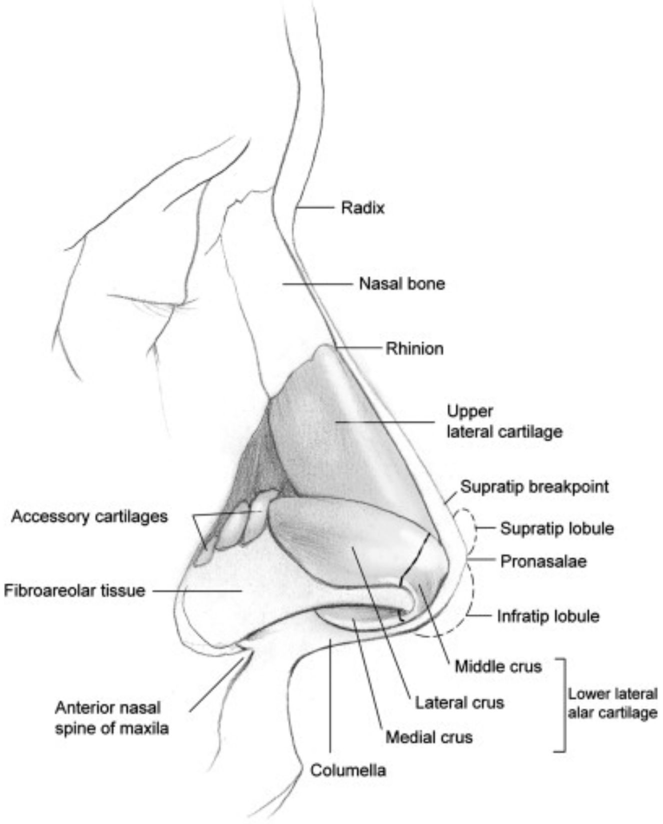

Figure 1.1 - Lateral view of the subdermal elements that form the structural and functional unit of the external nose (Stevens & Emam 2012)

The pair of *ossa nasales* lie on the superior dorsum of the nose and form the bony one third of the nasal ridge which is laterally confined by *processus frontalis maxillae* on both sides. The pair of *ossa nasales* lie on the superior dorsum of the nose and form the bony one third of the nasal ridge which is laterally confined by *processus frontalis maxillae* on both sides. Each nasal bone adheres superiorly to the *os frontale* and infero-anterioly to one of the paired *cartilagines nasi laterales (*upper lateral cartilages)(Rohrich 2018). The upper lateral cartilages form together with the cartilaginous septum internally and the nasal floor an "I-beam"-structure that supports the nasal dorsum and the pyramidal shape of the external nose.

The upper lateral cartilages and *cartilagines alares maiores* (the lower alar or lateral cartilages) together form the lower cartilaginous two thirds of the nasal ridge (Malaty 2018). The two cartilage pairs form a fibrous articulation at the lower edge of the upper lateral cartilage and the upper edge of lateral crus of the alar cartilage. The alar cartilage is U-shaped with two extensions. The medial parts, *crura mediales* (medial crus), define the form of the columella, whereas the lateral parts, *crura laterales* (lateral crus)*,* contribute to the structure of the nares.

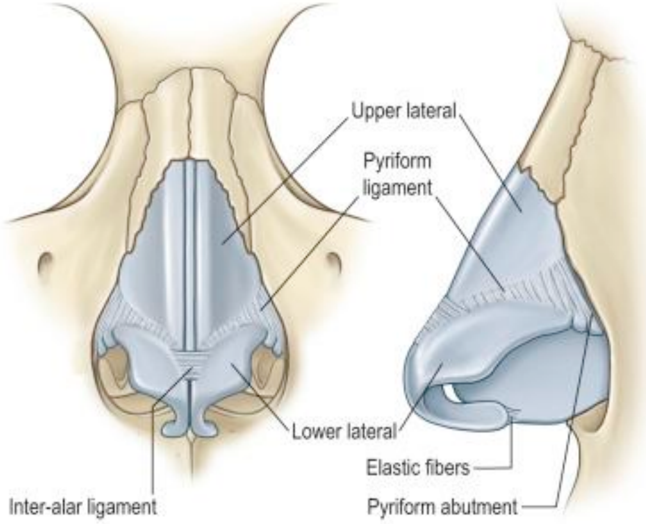

Figure 1.2 - Frontal (left) and lateral (right) view of the main nasal cartilages and ligaments (Rohrich 2018)

In order to provide stability and prevent deformation of the nose, the cartilaginous part of the external nose relies on the static support of the nasal septum and on a framework of interconnecting ligaments. The *ligamentum interalaris* (inter-alar ligament), also known as "Pitanguy's ligament", between the medial surfaces of the domes of the alar cartilages prevents widening and drooping of the nasal tip. The *ligamentum piriformis* connects the lateral crus of the alar cartilage and minor alar cartilages with the upper lateral cartilages (Rohrich 2018).

Musculature of the External Nose

Apart from interspersed fibro-fatty tissue, the external nose also features a highly-differentiated musculature. The main muscles are grouped into two categories. The first is the intrinsic nasal muscle group. It comprises *musculus nasalis* (nasalis muscle) and *musculus levator alae* which is an anatomical continuation of the nasalis muscle inferiorly. *Pars transversalis* of the nasalis muscle inserts at the edge of the upper lateral cartilage. Contraction of this muscle leads to the lateral expansion of the upper lateral cartilages increasing airflow within the nose. The functionality of the transverse part of the nasalis muscle is directly related to the functionality of the internal nasal valve (Stevens et al. 2012).

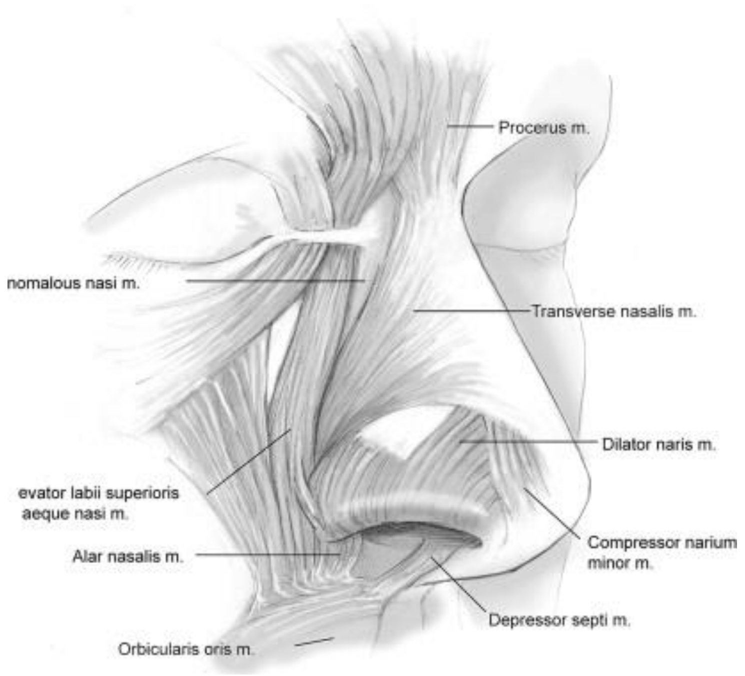

Figure 1.3 - Lateral view of the nasal musculature
(Stevens et al. 2012)

The extrinsic muscle group consists of *musculus procerus, musculus levator labii alaeque nasi,* the medial or angular division of the *musculus levator labii superioris, musculus depressor septi,* and *musculus orbicularis.* The muscle pairs of *levator labii* *superioris* and *levator labii alaeque nasi* provide nasal flaring when contracting. The performance of these muscles is related to the patency of the external nasal valve.

It is considered that the nasal musculature has a substantial impact on nasal airway patency through active contraction and passive static support of the nasal cartilages and soft-tissues of the external nose (Rohrich 2018).

Vasculature of the External Nose

As illustrated in figure 1.4 below, the external nose is mainly supplied by branches of *arteria facialis* arising from *arteria carotis* externa and, to a lesser extent, by *arteria ophthalmica* which gives rise to *arteria angularis*. All major nasal arterial branches lie above the muscles and nasal fascia.

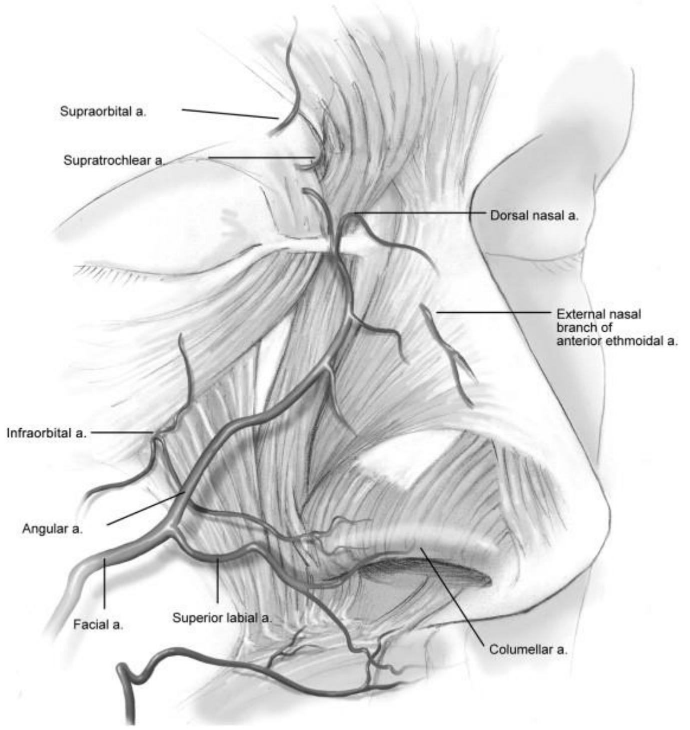

Figure 1.4 - Lateral view of the topographical anatomy of the nasal blood supply (Stevens et al. 2012)

The facial artery extends superiorly to connect with the angular vessel. While passing along the oral angle, inferior to the nose, *arteria labialis superior* branches off. The superior labial artery divides into numerous philtral branches that supply the ascending columellar arteries. *Arteria nasalis lateralis* derives from the angular artery and supplies the alar part of the nose and travels below the dermis. It gives off multiple so-called arcades that form anastomoses with the inferior ascending columellar arteries at the nasal dome (Rohrich 2018).

Sensory Innervation and Histoanatomy of the External Nose

The skin of the external nose receives its sensory innervation from the terminal branches of *nervus trigeminus.* Most importantly, *nervus ophthalmicus* and *nervus infraorbitalis.* The latter has multiple branches that provide sensation to the upper part of the lip, the alar base and the lateral nasal wall. The supratrochlear and ethmoidal branches of the ophthalmic nerve supply the superior nasal skin (Rohrich 2018).

In regard to histoanatomy, over the nasal bones and upper lateral cartilages the nasal skin is thin and freely mobile while that covering the alar cartilages is thick and adherent, containing many sebaceous glands. The nasal skin reaches into the nasal vestibule where it consists of hair follicles, providing fine hair called vibrissae, and stratified keratinized squamous epithelium that, passing through the vestibule towards the *cavum nasi proper*, gives way first to non-ciliated and then to ciliated respiratory epithelium. (Probst et al. 2018).

Anatomy of the Internal Nose

Anatomy of the Nasal Septum and Bony Nasal Cavity Proper

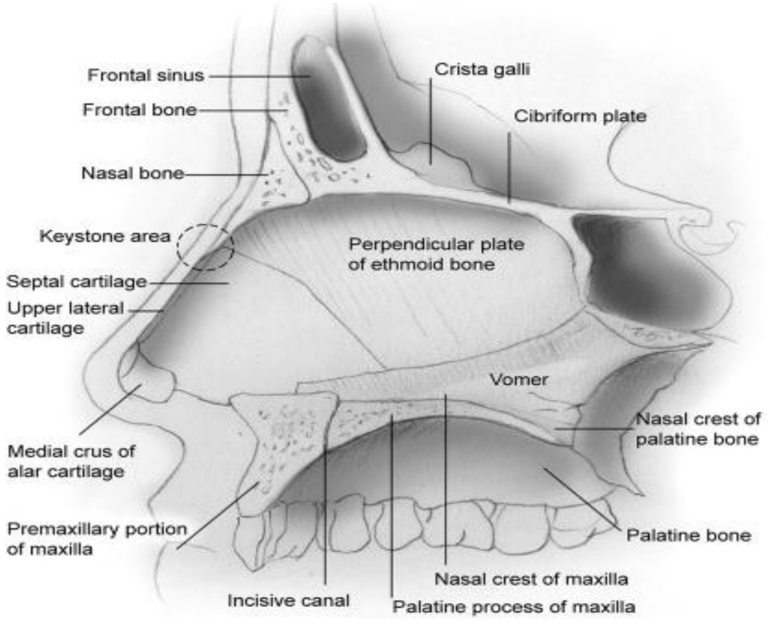

Figure 1.5 - Sagittal cross-section showing the structures forming the nasal septum and bony floor and roof of the nasal cavity (Stevens et al. 2012)

The nasal septum divides the internal nose into two nasal cavities that are laterally confined by the structures which make up the lateral wall of the nose and medially by the nasal septum (Guyuron 2012).

Antero-inferiorly, the nasal cavities begin at the nasal vestibule which is posteriorly bounded by the nasal valve. The bony anterior opening of the nasal cavities, called apertura piriformis, is formed by the maxillary bone laterally and inferiorly and superiorly by the nasal bone. Each nasal cavity proper is limited by the septum medially, the lateral wall laterally and by its roof and nasal floor (see figure 1.5). The nasal roof is grossly defined by three structures. The anterior sloping part is formed by the nasal bones, the horizontal part by *lamina cribrosa* (cribriform plate) of the ethmoid bone through which the *fila olfactoria* pass and the posterior down-sloping part is defined by *corpus sphenoidalis*. The relationship of these structures varies anatomically between each individual. The nasal floor in each nasal cavity is made up of *processus palatinus maxillae* (palatine process of the maxilla) in its anterior three-fourths and lamina horizontalis of the palatine bone in its posterior one-fourth (Lund et al. 2014).

The medial wall of the nasal cavity is defined by the septum. The nasal septum is cartilaginous and membranous caudally and bony cephalically (see above in figure 1.5). While the cartilaginous part is formed by the *cartilago septi nasi* (cartilage of the nasal septum), the bony part comprises the *crista frontalis* (crest of the frontal bone), *lamina perpendicularis* of *os ethmoidale*, the vomer, *crista sphenoidalis* (sphenoid crest) posteriorly, the crista nasalis maxillae and *lamina horizontalis* of *os palatinum* (Dhingra et al. 2014).

Anatomy of the Lateral Wall of the Nasal Cavity

The lateral wall of the nose bears three *conchae nasales* (turbinates), the inferior, middle and superior. Rarely a fourth so-called “supreme turbinate” is also present above the superior. The inferior turbinate consists of a separate bone that is attached to the medial wall of the maxilla. It has an uneven surface due to the impression of vascular sinusoids, to which the mucoperiosteum attaches (Lund et al. 2014).

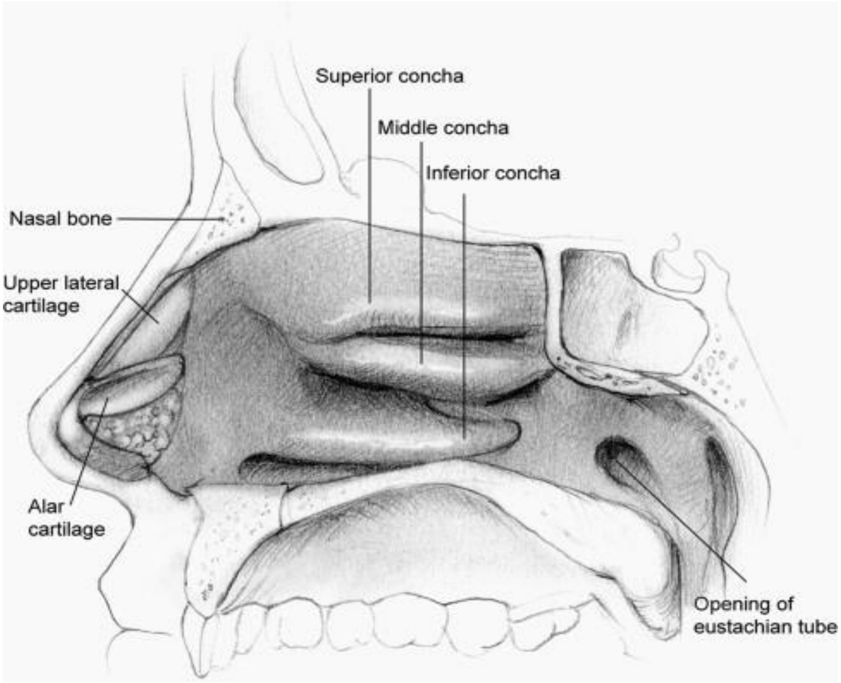

Figure 1.6 - Sagittal cross-section showing the anatomy of the lateral wall of the nasal cavity (Stevens et al. 2012)

The *ductus nasolacrimalis* (nasolacrimal duct) exits inferiorly to the turbinate at the opening of the *meatus inferior* where it forms a protective valve called “Hasner’s valve” (Dhingra et. al 2014).

Both, the middle and superior turbinate are part of the ethmoid bone. The middle turbinate is S-shaped and is fixed to the lateral wall by a bony lamella called *lamella basalis*. Its anterior part lies in a sagittal plane and is attached to the cribriform plate while its medial part is attached to the *lamina papyracea* of the medial orbital wall and lies in a frontal plane. The middle turbinate’s most posterior part runs horizontally and is partially attached to the *lamina papyracea* and the medial wall of the maxillary sinus. The middle turbinate forms the roof of the middle meatus. The middle meatus is the site where the ostiomeatal unit opens into the nasal cavity. It provides crucial drainage and ventilation for the maxillary sinus, frontal sinus and anterior ethmoidal cells. The superior turbinate is situated posteriorly and superiorly to the middle turbinate and bears olfactory epithelium on its medial surface. In practice, it forms an important landmark in identifying the location of the sphenoid sinus which lies medially to it. The superior meatus drains the posterior ethmoid cells in the area of the lateral wall of the nose covered medially by the superior turbinate. The nasal cavities communicate posteriorly through choanae with the nasopharynx (Probst et al. 2018).

The olfactory region of the nasal cavity proper is penetrated by *fila olfactoria* that pass down through the *lamina cribrosa* and appear macroscopically slightly paler than the respiratory mucosa. The trigeminal nerve is the main contributor to the sensory innervation. The lateral wall of the nasal cavity is innervated by *nervus infraorbitalis, nervus ethmoidalis anterior,* which both also innervate the corresponding medial part of the nasal cavity, and by branches of *ganglion sphenopalatinum* which supply the posterior two-thirds of the nose. The *ganglion sphenopalatinum* also provides parasympathetic fibers that control secretory function and cause capillary vasodilation. Corresponding vasoconstrictive sympathetic fibers are supplied by the *ganglion cervicale superior* and form the vidian nerve in the pterygoid canal (Dhingra et al. 2014).

The blood supply is divided into two main contributories, the *arteria carotis interna* and *externa*. Anteriorly, the blood supply is characterized by the confluence of four arteries: *Arteria ethmoidalis anterior* from the internal carotid artery and three branches of the external carotid artery, *arteria labialis superior*, *arteria palatina maior* and *arteria sphenopalatina*. This anatomical site is referred to as Kiesselbach's plexus, or Little's area. The drained blood of the nasal cavity either drains through the facial veins first or directly into the pterygoid and pharyngeal plexi or passes via the ophthalmic veins into the cavernous sinus and then into the sub-cranial venous plexi (Drake et al. 2018).

1.1.2 Anatomy of the Nasal Valve

The outer external nasal valve is formed by the lateral and medial crus of the lower lateral cartilage apically, baso-medially by the cartilaginous septum, maxillary nasal crest and nasal floor and infero-laterally by the fibro-adipose tissue of the alar lobule (Rohrich 2018). It communicates posteriorly with the internal nasal valve.

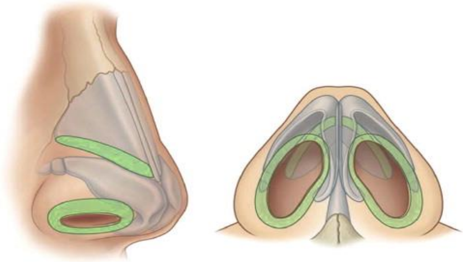

Figure 1.7 - Lateral and cranial view of the topographical relations of the external (outer green ring) and internal nasal valve (inner green ring) (Marin et al. 2009)

The internal valve, which is formed superiorly and laterally by the caudal end of the upper lateral nasal cartilage and its fibro-adipose attachment to the pyriform aperture. This valve is located at the level of the anterior end of the inferior turbinate which participates in airflow regulation through its erectile tissue.

While the inferior nasal turbinate has the biggest impact on airflow, septal and nasal floor erectile tissue may contribute to direct flow alteration (see black oval structures in figure 1.8). The internal nasal valve furthermore relates to the area called *ostium internum* which describes the transition zone between skin and nasal mucosa (Nigro et al. 2009).

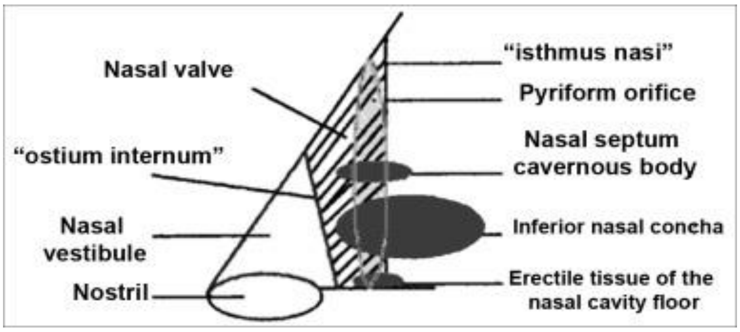

Figure 1.8 - Schematic relations of the internal nasal valve
(Nigro et al. 2009)

The internal nasal valve is anatomically defined by an angle between the upper lateral cartilages and the lower lateral cartilages laterally and the septum medially. This angle varies between 10° and 15° in Caucasians. Its shape and size depend on the individual's ethnicity with a range of up to 50° (Som et al. 2011).

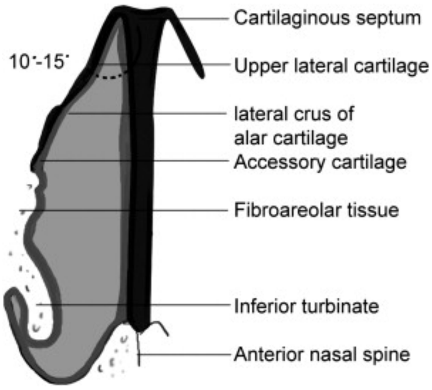

Figure 1.9 - Axial cross-section of the structures of the internal nasal valve
(Stevens et al. 2012)

Literature is still unclear in the correlation of the structures now defined as “ostium internum”, “internal nasal valve” and “isthmus nasi”, as they all take part in forming the nasal valve (Nigro et al. 2009).

1.1.3 Physiology of the Nose and the Nasal Valve

General principles

The nose, together with the paranasal sinuses, humidify, filter, warm, and perform olfaction during respiration (Jones 2001).

The physiological profile of the nose varies between ethno-geographical groups. There are three main groups characterized by nasal shape and size, namely leptorrhine, mesorrhine, and platyrrhine. These types correspond to differences in nasal height and width which also reflect in the angle of the internal nasal valve. These differences have been proposed to be evolutional adaptations to regional climate. The large and open platyrrhine nose has a high prevalence in warm-humid climates that have little need for efficient conditioning of air. The opposing narrow leptorrhine nose has evolved in harsher climate zones where the necessity of warming inspired air was more crucial (Eccles 2014). The mesorrhine (intermediate) category is most prevalent in the Asian population and reflects a blend of both other types.

The primary filtration site of the respiratory airway is the nose. The ability to filtrate air particles depends on their physical size, shape, and density and is expressed as its aerodynamic equivalent diameter (AED). Larger particles are mostly caught in the *vibrissae* (fine hair) of the nasal vestibule. Acceleration within the nasal valve and deceleration right after lead to turbulent flow which in addition favors particle deposition on nasal mucosa. During nasal breathing, most particles exceeding 15 µm AED (airflow equivalent diameter) are deposited in the upper respiratory tract. However, physiological or pathological mouth breathing may lead to the passage of larger particles into the trachea (Eccles 2014).

The humidity within the nasal cavity, which depends both on the humidity of the inspired air and the physiological humidification capacity of the nose, has a significant impact on filtration. Increased humidity leads to swelling of hygroscopic particulate matter which facilitates its chance of deposition. During to the humidification process, the nasal epithelium loses water to the inspired air. The nasal mucosa is cooled down as it transfers heat to warm the inspired air and for evaporation of water. During expiration, warm and highly humid air passes up through the cooler nasal airway where heat and water are partially reclaimed by the mucosa of the lateral wall and the paranasal sinuses (Eccles 2014).

Nasal heat exchange is strongly influenced by the filling and emptying of the venous sinuses. When the inspired air is cold, filling of the venous sinuses is increased in order to provide sufficient warming of the cold air before passing into the lower airways. Physiologically, these venous sinuses depend on sympathetic innervation.

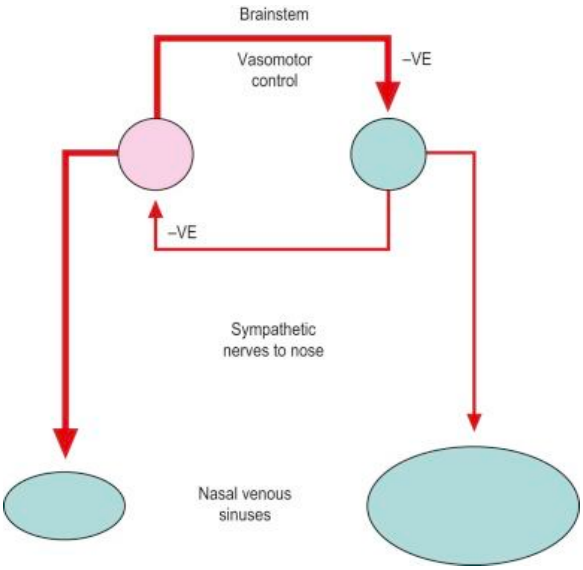

Figure 1.10 - Depiction of the circuit of the autonomous nervous system that regulates nasal venous sinus filling; "-VE" marks inhibition of neuronal activity (Eccles 2014)

Independently, the vasomotor response elicited by the brainstem may increase or decrease venous blood flow. It therefore exerts control over nasal airflow by nasal airway narrowing or widening and determines heat exchange between air and blood-filled nasal sinuses. This is thought to be the mechanism underlying the controversial "nasal cycle" phenomenon of alternating unilateral congestion and decongestion.

Lastly, the chemosensor function of the nose may indicate noxious chemicals and help to avoid them. It also contributes significantly to pleasure when eating and drinking or when exposed to pleasant odors. This function is not solely carried by the olfactory system but also by the trigeminal nerve. Chemicals can stimulate it directly or indirectly, eliciting sensations such as irritation, burning, tickling, piercing or the feeling of hot and cold (Eccles 2014).

Nasal Valve Physiology

In anatomy, the nasal valve is misleadingly divided into an external and internal valve. However, they act as one functional unit. Each nasal cavity has to be regarded as its own physiological entity. Simplified, each side can be seen as a tube that enables passage of air into- and out of the lower respiratory tract. Yet in reality, its specialized inner anatomy modifies the air stream in a way that is unique to every individual.

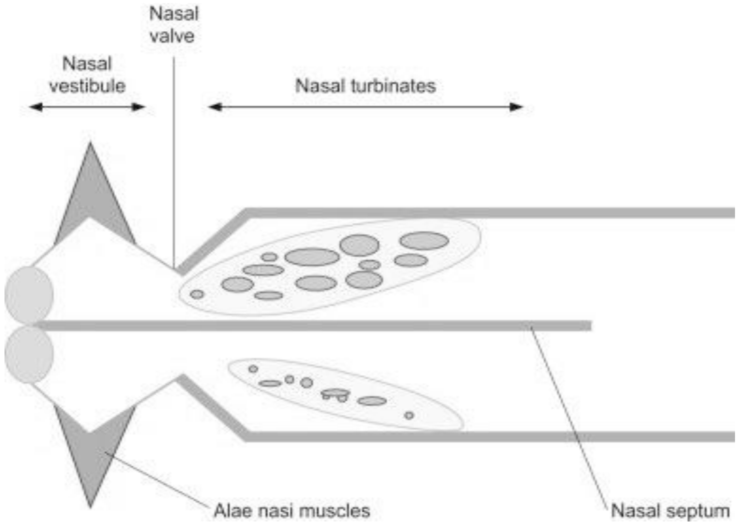

Figure 1.11 - Simplified scheme of the nasal airway. The nostrils are depicted as two ovals (on the left), whereas the nasopharynx opens postero-inferiorly to the septum (to the right). (Eccles 2014)

Nasal valve physiology depends strongly on its anatomical configuration, including its cartilaginous, muscular, soft tissue and mucosal components. Pathological changes of aforementioned structures maybe lead to a compromise of nasal valve function.

When inspiring, the stream of air travels from the vestibule through the nasal valve, the narrowest airway passage, into the nasal cavities. Inspired air reaching the nasal valve is aerodynamically in a state of laminar flow. The term “laminar flow” describes an air stream pattern that consists of parallel, mostly undisturbed air stream layers. When passing through the nasal valve the flow is modified to change into the state of turbulent air flow (Probst et al. 2018). This effect is further amplified by the nasal turbinates, mainly the inferior turbinate.

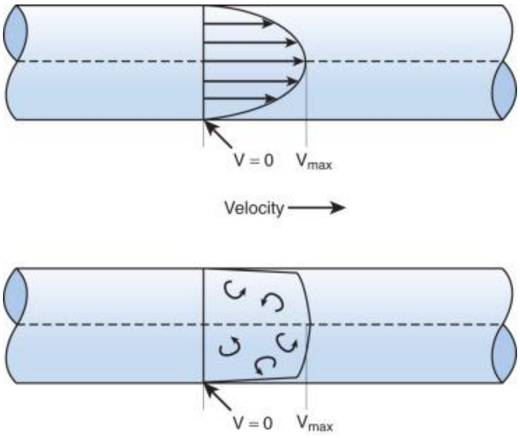

Figure 1.12 - Schematic showing airflow dynamics in laminar flow (upper) and turbulent flow (lower); V - velocity, Vmax - maximum velocity (Doyle 2018)

The changes in flow dynamics across the nasal valve a depicted in figure 1.12. The upper graphic represents flow in the nasal vestibule and the lower graphic in the nasal cavity. The pre-valvular airflow is characterized by a parabolic velocity profile with an increased median peak velocity. Post-valvular airflow has a flattened profile with turbulent airstream layers. Its velocity is almost equal across the lumen, except for the edges closest to the nasal wall. If laminar flow exceeds its critical velocity, it becomes turbulent (Doyle 2018).

The internal nasal valve is the narrowest passage of the upper respiratory airway and, thus, the structure exhibiting the highest airflow resistance. The importance of its anatomical characteristics can be underlined by the Hagen-Poiseuille law of fluid kinetics:

$$R = \frac{8\eta l}{\pi r^4}$$

R – resistance, r - radius, η - fluid viscosity, l - length of the tube

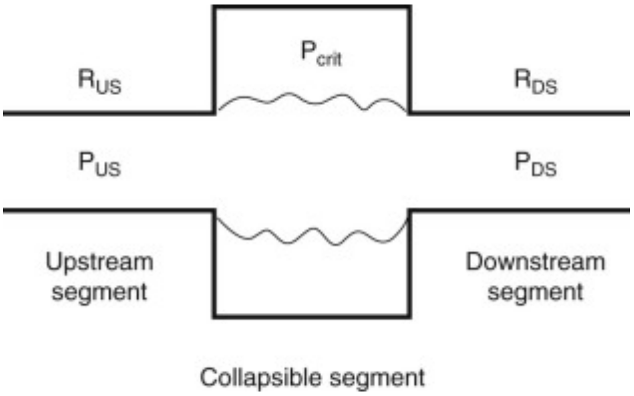

Figure 1.13 - Scheme of simplified airflow across the nasal valve;
Pcrit - threshold of pressure needed to collapse the segment, US - upstream segment,
DS - downstream segment, P - intra-luminal pressure, R structural resistance
(Tal 2014)

Often referred to as the "Fourth power law", it illustrates the dependence of resistance on the radius of the passage way (Harten 2011). In regard to the nasal valve, according to the equation above, a decrease of the radius by only 10% would already lead to an increase in resistance by approximately 50%.

The internal nasal valve is not only the narrowest part, but also an elastic segment of the upper airway. In order to understand figure 1.13, one must know that nasal airflow at the site of the nasal valve also complies with Bernoulli's principle of fluid dynamics. Bernoulli's principle defines flow through a tubular structure as constant at the two ends. This principle is also applicable to the nasal airway. Flow is held at a constant level during inspiration by increasing physical work. Taking the law of Hagen-Poiseuille into consideration (see equation above), Bernoulli's principle describes the phenomenon in which flow increase momentarily to overcome a segment of decreased diameter, in this case the nasal valve. The acceleration in flow leads, paradoxically, to an intra-luminal drop in pressure.

The in figure 1.13 illustrated Pcrit is the external pressure needed to trigger a luminal collapse of the segment. If Pcrit exceeds the pressure within the nasal valve, it collapses, causing a momentarily and drastic increase in airway resistance (Tal 2014).

The physiological function of the nasal valve can be likened to a Starling resistor, in which the degree of collapse can be adapted (Knowlton & Starling 1912).

1.2 Diagnostic Evaluation of the Nasal Valve

The diagnostic evaluation of the nasal valve is part of the investigations performed in patients with nasal obstruction. Most tests however lack specificity towards valvular disorders. Therefore, it remains difficult to assess the relation between the clinically present obstruction and the functionality of the valve.

Looking back in history, initially two clinical tests for nasal obstruction were gaining attention during the turn of the 19th century. One was the “hum test” by Spiess in 1902, when he suggested that humming of the patient while alternatingly closing one nare may help identifying obstruction of the nasal airway on one side. The other was introduced by Zwaardemaker and called “hygrometry test” in 1889 (Uddströmer 1940). This was a functional test using a cold mirror placed under the nose to estimate the degree of airflow obstruction during exhalation by measuring the diameter of the fog that was produced.

At present day, nasal valve assessment aims at identifying nasal valve collapse which can be of static or dynamic nature. Whereas static valve collapse is commonly pathological, dynamic collapse has to be set into relation to the present nasal airflow. If a certain threshold of flow is surpassed, physiological nasal valve collapse occurs. Therefore, premature or below-threshold dynamic collapse would be pathological.

1.2.1 Current Diagnostic Techniques

At the present time, the range of applicable diagnostic tests that analyze and characterize nasal valve function is limited and predominantly physician-dependent. As a consequence, an assessment relies heavily on non-specific diagnostic tests for nasal obstruction and the physician’s adequate evaluation. Furthermore, patient questionnaires such as the Nasal Obstruction Visual Analogue Scale (NO-VAS) are still a cornerstone in recognizing nasal obstruction prior to any diagnostic tests.

In practice, the motility of the nasal valve is assessed by the physician as a part of a standard rhinological diagnostic work-up. Preferably, it should be performed at all physiological stages of the nasal valve, thus, during normal breathing and deep inhalation and exhalation.

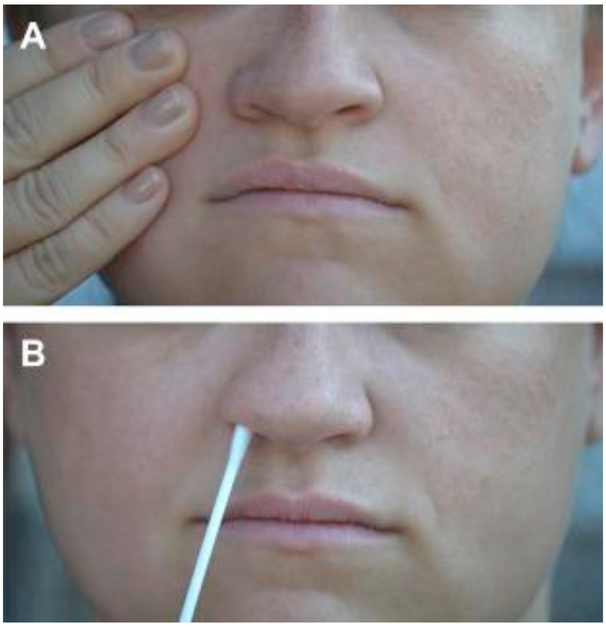

Figure 1.14 - Cottle manoeuvre (A) and modified Cottle manoeuvre (B)
(Sowder et al. 2017)

Patients undergo external visual inspection and palpation which may already reveal potentially obstructive nasal conditions. Anterior rhinoscopy is then performed to visualize the nasal airway. The focus hereby lies on signs of pathological collapse, the condition of skin and mucosa within the nasal airway, the configuration of the inferior turbinates and the nasal septum and the presence of obstructing masses such as tumors or polyps (Rohrich 2018). All of these may interfere with the functionality of the nasal valve.

The Cottle manoeuvre and the modified Cottle manoeuvre are often useful in confirming nasal valve dysfunction. The principle of both is to prevent valvular collapse mechanically in order to produce a temporary and confirmatory absence of airflow obstruction. In the Cottle manoeuvre, the patient’s upper cheek is pulled laterally which is generating additional tension within the ipsilateral nares decreasing the range of motion of the nasal valve. The modified Cottle manoeuvre uses a cotton-tipped applicator that is placed inside the nose against the lateral wall at the site of the nasal valve preventing its collapse during breathing.

However, a positive result of each manoeuvre is non-specific and can be appear with other causes of obstruction, such as septal deviation or inferior turbinate hypertrophy in absence of nasal valve dysfunction (Sowder et al. 2017).

Targeted diagnostic tests aiming to assess nasal function may be divided into two categories. The first being investigations of the nasal airstream and its characteristics such as humidity and temperature. The second category includes diagnostics directed towards the nasal mucosa. Within this investigation spectrum falls also the analysis of ciliary activity and mucosal blood flow which is currently making its way into clinical practice via photonic methods, as for instance optical coherence tomography (OCT) or other novel spectroscopic techniques.

It is paramount to understand the physiological concept of the nasal airstream which is determined by the flow (flux) and the precipitating differential pressure between the nares and the choanae (Eccles 2014). Thus, the most accurate diagnosis lies in the trinity of:

- Determination of pressure and flow and its mutual relation to get quantitative and global information about the degree of obstruction / resistance of the individual nasal air stream
- Visualization of the nasal air stream by Computational Fluid Dynamics (CFD) for the topical information of anatomical structures in respect to the nasal resistance
- Investigation of elastic structures and the resulting variations of the nasal airstream during breathing, leading mainly to valve phenomena

The step towards including diagnostics targeting elastic nasal structures means the transition from a static to a dynamic airway diagnosis.

Importance of rhinomanometry and 4-phase-rhinomanometry

The international RIGA consensus conference on nasal airway function tests, held in Riga on the 2nd of November 2016, agreed that rhinomanometry remains the most important basic nasal function test. However, “classic” rhinomanometry does not fulfil the expectations of state-of-the-art diagnostics. Therefore, it was recommended to introduce 4-phase-rhinomanometry (Vogt et al. 2010) with its new parameters as a standard investigation method.

The development of active anterior rhinomanometry (AAR)

In 1965, the publication “Die klinische Bedeutung der Nasenwiderstandsmessung” by H. Masing (Masing 1965) emphasized the importance of nasal resistance in the objective assessment and diagnosis of nasal obstruction. Three years after, in 1968, Cottle introduced passive anterior rhinomanometry (PAR) (Cottle 1968). With the advance of computer technology, AAR came finally within reach (Clement et al. 2014).

In 1984, the “International Standardization Committee for the Objective Assessment of the Upper Airway” as a group of the European Rhinologic Society published standardizing recommendations for rhinomanometric measurements (Clement et al. 2014). These included the graphic realization of the data in four quadrants displaying both nasal cavities in inhalation and exhalation, mirrored at the Y-axis. The flow is plotted on the Y axis and the pressure on the X axis. The committee also agreed on the SI units being cm3/s for the flow and Pa for the pressure gradient.

The modern standard of 4-phase rhinomanometry

4-phase rhinomanometry comes with a range of main advantages compared to classic rhinomanometry (Vogt et al. 2010)

1. Analyzing the entire breathing cycle instead of single-point analysis
2. Deriving directly measured parameters as indicators for the dynamics of nasal breathing instead of estimated values from the single-point analysis
3. Significant correlation between the logarithmic transformation of the measured parameters and the sensing of obstruction

4. Inclusion of the dynamics of the nasal valve and its visualization in the depicted loops

Analyzing the wave instead of an incorrect regression line was first published by Vogt et al. as “High Resolution Rhinomanometry” and after the consensus conference of the ISOANA in 2003 renamed as *“4-Phase-Rhinomanometry”(4PR)* (Vogt et al. 2010).

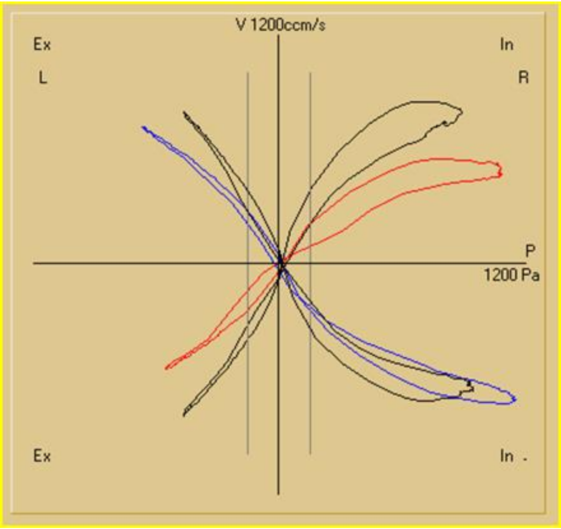

Figure 1.15 – Typical graph of 4-phase rhinomanometry based on the principles of the recommendation for standardizing rhinomanometry in 1984 (see page 22)
(Vogt et al. 2010)

The phase shift between flow and pressure gradient observable at the peak of the loop in figure 1.15 during inspiration is caused by the compressibility of the air and inertia of the airstream and the elasticity of anatomical structures, such as the nasal valve, and is also called nasal valve phenomenon.

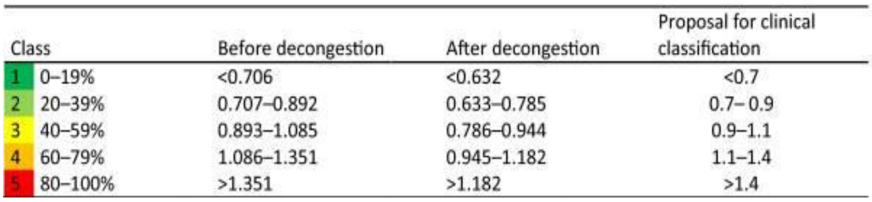

Class		Before decongestion	After decongestion	Proposal for clinical classification
1	0–19%	<0.706	<0.632	<0.7
2	20–39%	0.707–0.892	0.633–0.785	0.7– 0.9
3	40–59%	0.893–1.085	0.786–0.944	0.9–1.1
4	60–79%	1.086–1.351	0.945–1.182	1.1–1.4
5	80–100%	>1.351	>1.182	>1.4

Figure 1.16 – Proposed classification of logarithmic effective resistance for 4-phase rhinomanometry
(Vogt et al. 2016)

Acoustic Rhinometry

Acoustic rhinometry (AR) is simple and painless and yet one of the major diagnostic methods used in objective analysis of nasal patency. With the help of acoustic waves that are induced from its sensor head (see figure 1.17) at the level of the vestibule, it can give detailed information about the spatial environment of the nasal cavity in the shape of a two-dimensional image. Thus, being able to identify narrow segments which may be the cause of nasal obstruction. It however cannot give proper information on nasal respiratory function.

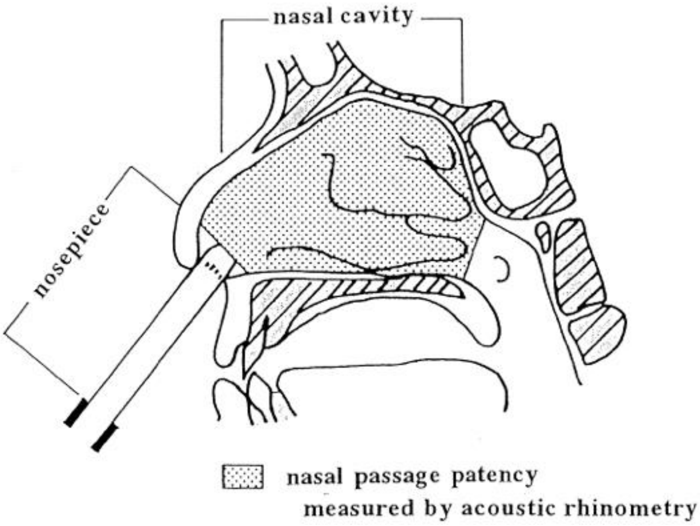

Figure 1.17 - Schematic showing the application of the acoustic rhinometer
(Miyahara et al. 1998)

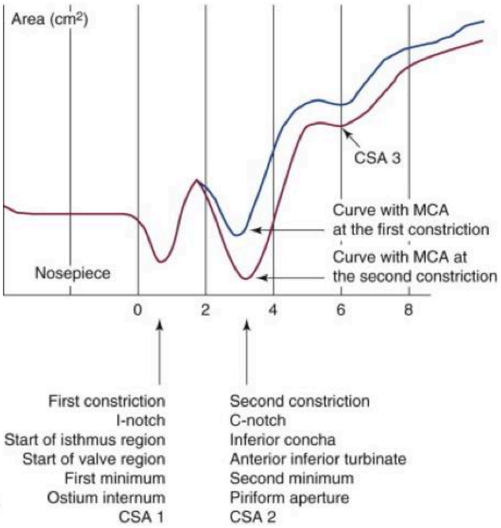

Figure 1.18 - Standard acoustic rhinometry graph reflecting anatomical sites of the nasal airway
(Pallanch & Jorrisen 2015)

The measurements are carried out prior to and after nasal decongestion giving a general picture of the impact of mucosal congestion and, additionally, of anatomical variances affecting the intranasal cross-sectional diameter in the decongested nose. (Pallanch & Jorrisen 2015).

Such anatomical variances are also shown in respect to the nasal valve. Sometimes the minimal cross-sectional area (MCA) matches the nasal valve and in others the head of the inferior turbinate (see figure 1.18). To clarify the exact anatomical site of the MCA, decongestion is crucial as it relieves the swelling of the anterior inferior turbinate but has little influence on the nasal valve. AR also measures various cross-sectional areas (CSAs) at certain distance intervals within the nasal cavity.

Anatomical sites commonly registered in acoustic rhinometry:

- CSA1 - the internal nasal valve approximately 0.75 cm from the nostril
- CSA2 - the head of the inferior turbinate approximately 2 cm from the nostril
- CSA3 - is correlates the head of the middle turbinate and the caudal part of the inferior turbinate approximately 4 cm from the nostril

The narrowings at CSA1 and CSA2 are occasionally labeled I-notch, for isthmus nasi, and C-notch, for concha inferior, respectively (Pallanch & Jorrisen 2015).

For acoustic rhinometry as well as for rhinomanometry, both sensitivity and specificity are higher regarding the prediction of post-operative satisfaction than is the case for anterior rhinoscopy alone (Pirila & Tikanto 2009).

Peak Nasal Inspiratory Flow (PNIF)

Implemented from pulmonological functional testing, PNIF is a simple, inexpensive and non-invasive technique that helps to evaluate the patency of the nasal airway. The peak flow during inspiration is measured which, if below threshold, may indicate nasal obstruction. Additionally, PNIF is notable to distinguish between obstructive and other causes of decreased flow, such as inflammatory or pre-nasal (Texeira et al. 2011).

Figure 1.19 - Peak Nasal Inspiratory Flow Meter (Texeira et al. 2011)

However, this measurement regards the nasal airway as one unit and does not differentiate trans-nasal pressure gradients. Therefore, it is highly susceptible to compliance of the patient and adequate instructions by the examiner (Chandra et al. 2009). In spite of its wide spread use, peak nasal inspiratory flow does not represent a realistic nasal function test since the nasal peak flow, i.e. the maximum inspiratory flow is physiologically used to narrow the nasal wings to clean the nose from mucus. Thus, any information about the elasticity or function of the nasal valve is unattainable.

1.2.2 Prospective Techniques

Computational Fluid Dynamics (CFD)

Based on computer tomography images of the upper airway, software is able to produce a three-dimensional reconstruction of the anatomical surface. In order to be able to simulate actual airflow, a mesh with approximately 4 million tetrahedral cells is generated. A driving pressure is then assigned by the physician (Pallanch & Jorrisen 2015). This novel method may play a key role in understanding nasal biophysics.

It remains a challenge to understand the vast variety of physiologic airflow patterns and to establish reliable parameters to correlate the produced patterns to nasal obstruction. As seen in figure 1.20 below, different results for non-pathologic airways can also be seen for Caucasians, Chinese and Indian individuals.

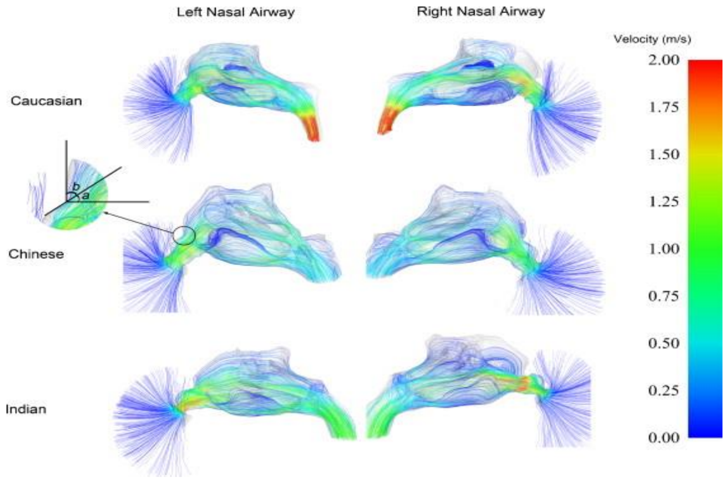

Figure 1.20 - Results of computational fluid dynamics for different ethnic groups (Jian et al. 2011)

The necessary computation resources for CFD have become more widely available decreasing the costs for data analysis and management. This has led in recent years to a surge in the practical application of CFD. A newly founded international society (SCONA) is now engaging into elaborating respective standards and promoting a broad introduction of CFD into clinical practice.

The here presented technical tests and developments are a part of the Austrian-German project “Rhinodiagnost” which is working within this context.

1.3 Therapeutic Approach

As mentioned above, the contribution of the nasal valve to the physiology, and conversely, dysfunction of nasal breathing is still often underestimated. Consequently, we must analyze the nasal valve as an entity in itself, but also the potential impact further understanding may have on rhinoplasty, functional and cosmetic, as a whole.

A first-line option for nasal obstruction, especially if lateral nasal wall insufficiency is suspected, is the use of nasal dilators. Common types include external strips traversing the nasal ridge and internally placed stretchers.

Figure 1.21 - Left: External nasal dilator; Right: Internal nasal dilator
(l.: Dinardi et al. 2017; r.: Dinardi et al. 2016)

Two studies performed at the Sports Complex of the Pontifical Catholic University in Belo Horizonte, Brazil, showed a vast improvement of cardio-respiratory performance in the young. This displays the magnitude of importance and the potential impact nasal valve dysfunction.

In recent years, minimally invasive options such as the “Latera implant” made by Spirox Inc. can be placed percutaneously through the vestibular skin on each side or the affected side of lateral wall collapse in an office setting. It is made of an absorbable polymer that will resorb completely within 18 months. The fibrous capsule that has formed around the implant during the wound healing process remains even after resorption giving possibly a longer-lasting benefit (Samra et al. 2018).

However, for those who seek a permanent and lasting relief without the use of gadgets such as nasal dilators, a surgical treatment may be applied.

Radiofrequency-induced Thermotherapy

For this technique a radio-frequency probe is applied which induces finely controlled tissue necrosis at the site of the nasal valve area internally. This results in an overall reduction of tissue volume in the treated area.

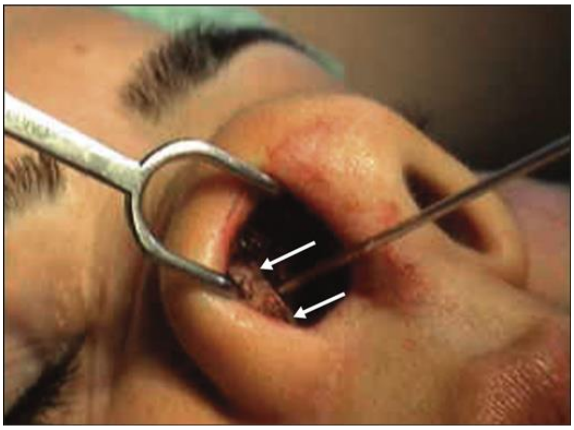

Figure 1.22 - Setup of the procedure with a retractor on the left and the radiofrequency probe on the right; white arrows indicate the site of application (Seren 2009)

In a prospective study performed in Turkey in 2009, 28 patients underwent this procedure to treat nasal obstruction due to inspiratory nasal valve collapse. The efficacy was assessed using a visual analogue scale for nasal obstruction. All participants were given the questionnaire before and 16 weeks after the treatment (Seren 2009)

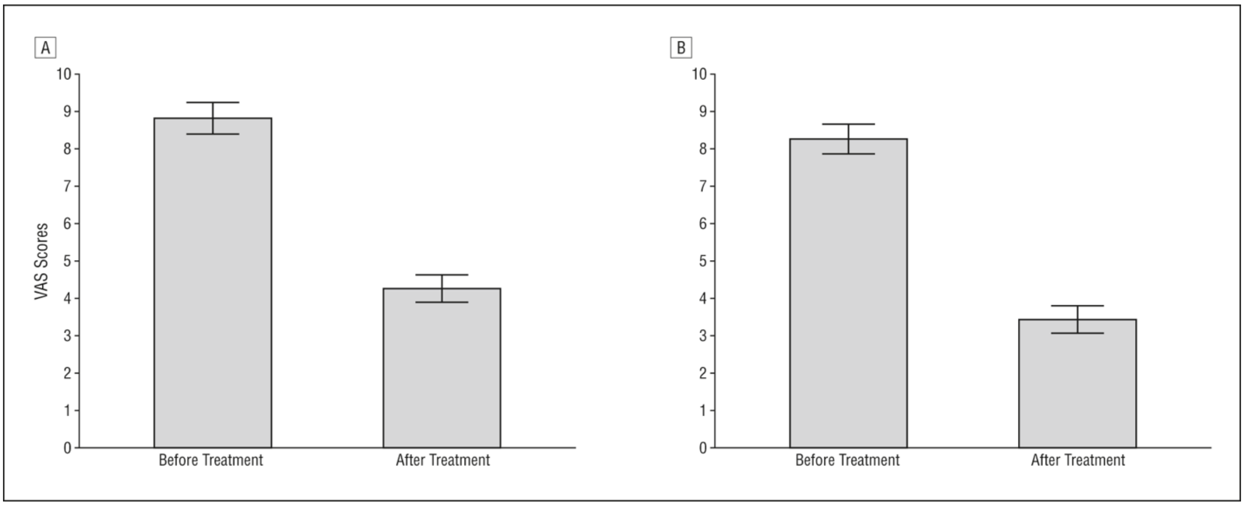

Figure 1.23 - Results of questionnaire showing the impact of nasal obstruction on the participants on a scale from 1 to 10 before and after the treatment; A: Right nostril, B: Left nostril (Seren 2009)

One must however remark, that tissue reduction may not be an adequate approach in patients that suffer from a dynamic nasal valve collapse due to a significant change in valve elasticity. In these patients, thermotherapy may only give partial or short-lasting relief.

Upper Lateral Strut Grafting

This procedure is one of several techniques that underlie the principle of restoring an adequate physio-anatomical state of the external nose, notably the cartilaginous structures. That may also include plasty of the prevalent cartilages and suturing to provide stability of the lateral nasal wall. These surgical grafts, usually autogenous cartilage, are implanted to address weak or malpositioned *crura lateralia* of the *cartilagines alares maiores* and increase nasal tip projection in aesthetic surgery. Furthermore, the placement of strut grafts can potentially decrease collapse of the nasal valve (Neligan & Buck 2014).

Spreader Grafting

The part of the nasal valve referred to as the "internal nasal valve" belongs to the most frequently, concomitantly altered areas in septorhinoplasties, indirectly and directly. Spreader grafts are harvested from septal or costal cartilage.

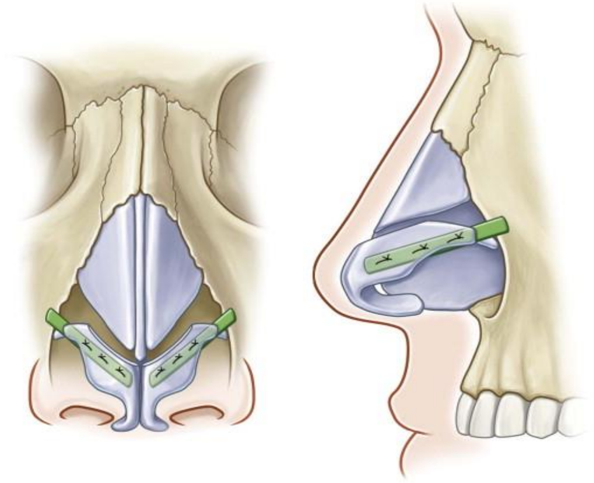

Figure 1.24 - Frontal (left) and lateral (right) view of the graft placement in relation to the nasal cartilages (Neligan & Buck 2014)

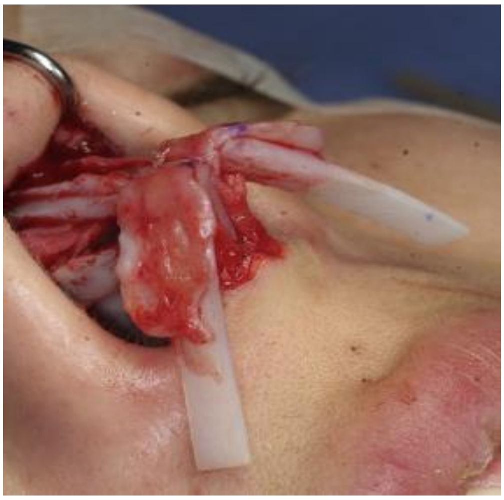

Figure 1.25 - Image taken of the strut grafts attached to the crura lateralia (Samra et al. 2018)

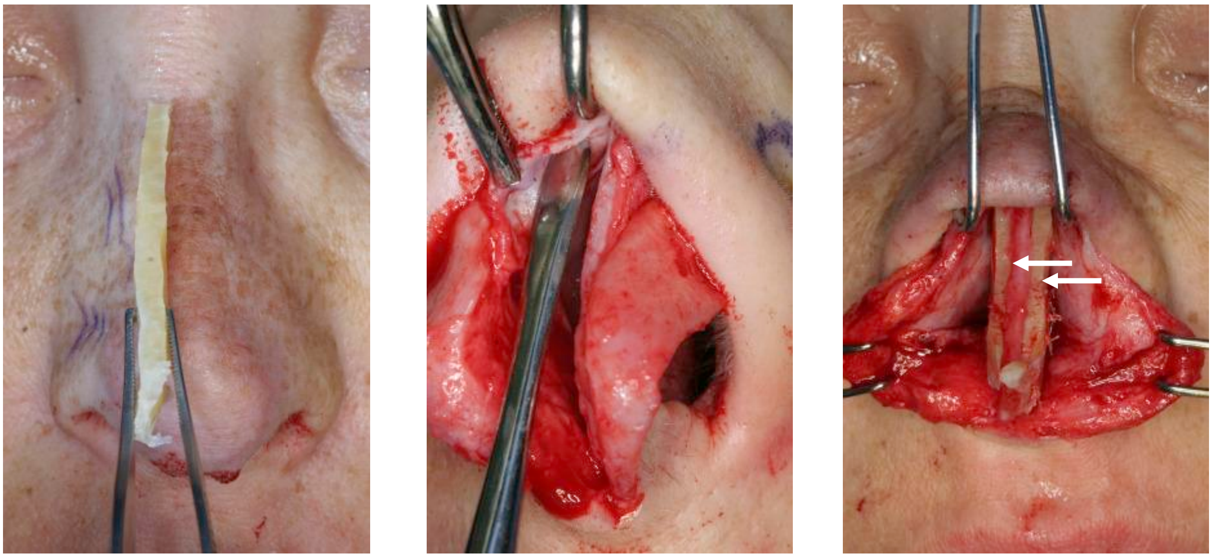

Figure 1.26 - Spreader graft implantation; Left: Costal spreader graft; Middle: Preparation of a graft pocket; Right: Bilateral spreader grafts in place (white arrows)
(Samra et al. 2018)

The grafts are either positioned into a submucosal pocket at the apex of the nasal valve or between the *cartilagines nasi laterales* and *cartilago septi nasi.* Hence, the apical part of the nasal valve is widened and stabilized preventing an early complete valve collapse.

As stated previously, the nasal valve has a large impact on the patency of the nasal airway. Likewise, other anatomical structures influence the function of the valve. These include among others the septum and inferior turbinate. Any surgical procedures on these structures should be performed knowing the physiological consequences they may have on the nasal valve.

1.4 Quantitative measurement of the nasal valve motility

The nasal valve is motile during nasal breathing. Obtaining an objective measurement technique remains a challenge to this day.

In order to understand its physiology and role in disease, we need to measure the exact degree of displacement of the valve. Since its motility is only visible to the naked eye during deep forced nasal inhalation or exhalation, highly sensitive instruments are required in normal, physiological breathing.

In theory, two groups of techniques seem viable to obtain quantifiable data. The first group is the video-assisted analysis and the second is the use of displacement gauges. The latter measures displacement, representing a change in position of an object with respect to a reference.

1.4.1 Displacement gauges

Displacement gauges are divided into contact and non-contact types. Contact type gauges include strain gauges which were successfully used to obtain unquantified measurements from the nasal valve by Liga Akmenkalne et al. in 2018 (Akmenkalne et al. 2018).

Non-contact displacement gauges include optical, capacitive, Eddy current, ultrasonic and laser focus sensors. Non-contact sensors offer the great advantage of being wear-free and thus potentially reusable.

Strain Gauges

Strain gauge sensors transform strain applied to it into a proportional change of resistance, and thus allowing to infer the amount of stress and displacement. The electrical resistance within the conductor changes depending on the degree of force that is directed towards the sensor within the limits of its elasticity.

Therefore, the material chosen for the gauge has a substantial influence on its performance and is compared by its gauge factor, Gf.

$$Gf = \frac{\Delta R \;/\; R1}{\varepsilon}$$

Gf = Gauge factor
ΔR = Change of resistance
R1 = Baseline resistance
ε = Applied strain

Inherent to this mechanism of sensing, the output of strain gauges is not linear. The sensor sensitivity is the greatest at median strain levels while it decreases exponentially at the extremes of the pressure range. This requires a careful and adapted selection of the material, thickness and bonding technique. If the applied strain ε exceeds the elasticity threshold of the gauge it may lead to an incomplete or incorrect return to zero after the strain was applied. This error is called hysteresis. Another common issue with strain gauges is the zero shift with a change of temperature which can be compensated by using additional resistors, if necessary. Within the medical setting of measuring the nasal valve motility, significant temperature changes are not expected (Hoffmann 1987).

Capacitive Sensors

These sensors utilize the physical principle of capacitance. It is based on the ability of a capacitor to store an electrical charge. In a parallel plate capacitor, the capacitance is calculated by $C = Q / V$.

Capacitance (C) is related by the stored charge (Q) at a given voltage (V). Displacement can thus be detected by generating an electric field between both plates and measuring its attenuations (Harten 2011).

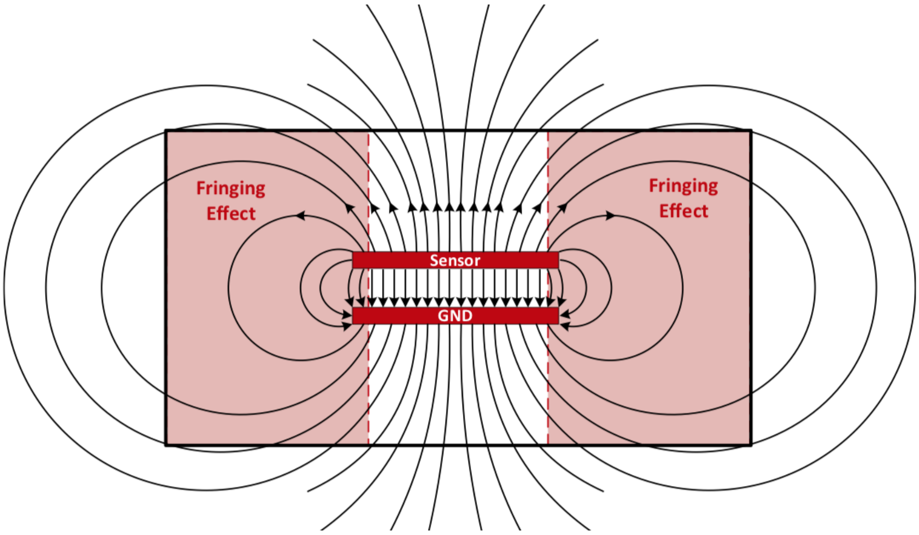

Figure 1.27 - Parallel plate capacitor showing the sensor plate and the ground conductivity plate (GND) (Wang 2014)

Capacitive sensing only needs one capacitive sensor plate, whereas the grounded (GND) plate can be represented by a variety of materials, e.g. metals, wood and also human skin.

The electric field lines start from the higher voltage potential charged plate, the sensor plate, and end at the lower voltage potential charged plate, the GND (ground conductivity plate), in our measurements, the external surface of the skin above the nasal valve. The fringing effect shown in the large red squares on both sides of the plates in figure 1.27 becomes more relevant for larger distances between the plates but may affect the accuracy of the measurement.

$$C=\frac{\varepsilon_0\varepsilon_r A}{d}$$

Capacitance - C, dielectric constant of air - ε_0, dielectric constant of the target material - ε_1, surface area of capacitor plates - A, distance between capacitor plates - d

This sensor technique is heavily influenced by the dielectric constant (ε_1) of the target object which is determined by the target material. Therefore, accuracy of this type of distance measurement decreases sharply with contamination of its environment. In medical practice, it is unrealistic to routinely achieve an adequately electrical-pollutant-free environment to ensure high-quality diagnostic data.

Inductive Sensors

Inductive sensors, or Eddy-current type sensors, use, in contrast to conductive sensors, a magnetic field to determine the proximity of a target object. In this measurement technique, the target object is a conductive, ferrous metal. The inductive sensor consists of an induction loop that generates a magnetic field when an electrical current is applied. An object within this field, for example our target object, will then alter the sensor’s magnetic field through its conductivity. The closer it gets, the greater it’s conductivity within the magnetic field (Harten 2011). This impact is also referred to as Eddy current.

To utilize this technique for our aims, it is necessary to fixate a small metal platelet to the skin on the lateral external nasal wall in order to create a physically measurable target object. Opposite to conductive sensing, this technique is usable in versatile and contaminated environments as the sensor only reacts to the proximity of the metal platelet.

Ultrasonic sensors

Ultrasonic distance sensors are based on the pulse-echo method. The ultrasonic probe sends off a sound wave which is reflected by the next obstacle, our target object. The reflected sound wave then arrives back at the probe which now serves as a wave sensor. The time passed between sending and receiving the signal is then used to determine the distance to the object:

$$d\ (t) = 0.5 \cdot c \cdot \Delta T$$

Distance (d) dependent on time (t), sound wave velocity (c), Time interval in between sending and receiving the signal (ΔT)

The value 0.5 is included since the recorded time interval includes both, the time passed to reach the object and the time needed to return to the probe.

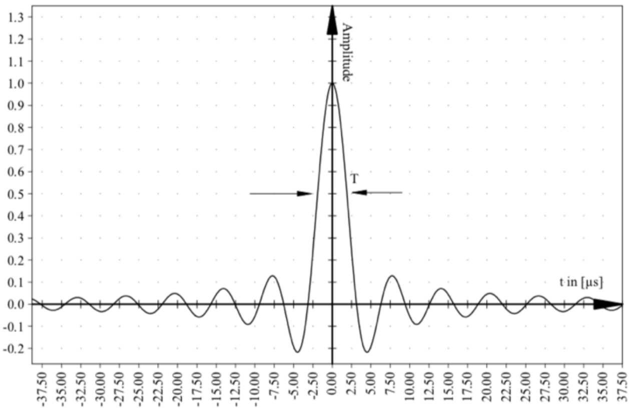

Figure 1.28 - Relative changes in amplitude before, during and after (ring-down time) the sound wave generation by the probe (Stehning 1999)

Ultrasonic distance measurement however also has its limitations. If the distance to the object reaches a critically close range, for example less than 10mm, the time needed to create the signal and the time that will pass until the signal returns are almost of equal values (see figure 1.28).

Since the probe needs a certain time to cease swinging after creating the signal, the so-called ring-down time, this will interfere with the recorded time interval and reduce the accuracy of the measurement dramatically (Stehning 1999).

Optical Sensors

Distance measurement is also possible in applied optics. It is based on the same physical principle as ultrasonic sensors. A light source sends a uni-frequent wave that is then reflected by the target object (Harten 2011). The distance is deducted from the time that has passed until the reflected signal is received. Contrary to the ultrasonic probe, modern-day optical sensors are capable of measuring close-distance mobile objects. Various subtypes of optical sensors vary in the wavelength of light utilized and the modality by which the light beam is created.

1.4.2 Camera-Assisted Analysis

The principle of this technique is based on camera-assisted observation of the nasal valve during normal, physiological breathing. Hereby a camera is introduced into the nasal vestibule. In potential camera-assisted analysis, one has to keep in mind both static, such as the septum, and dynamic elements, such as the lateral wall of the nasal valve.

The camera-assisted assessment was used as a diagnostic tool in “The internal nasal valve: a validated grading system and operative guide” by Patel et al. (2018). The study was performed on patients who underwent primary external functional septorhinoplasty for nasal obstruction. The grading system was applied by anterior 0°-rhinoscopy before and after operational intervention in a blinded, independent process by 3.

The different grades were based on the degree of visualization of the middle turbinate at the level of the inferior turbinate within the internal nasal valve. A higher degree signified a greater level of obstruction.

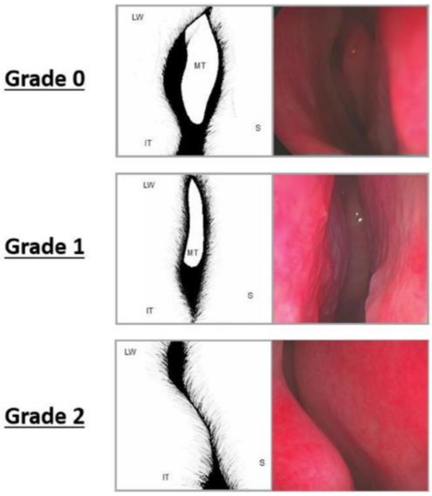

Figure 1.29 - Grading system applied during the study by Patel et al. (2018). Right column shows rhinoscopic view of the internal nasal valve. Septum (s), Middle turbinate (MT), Lateral wall (LW), Inferior turbinate (IT) (Patel et al. 2018)

Patel et al. (2018) related the static, non-dynamic component of the nasal valve to its functionality. This is further limited by lack of accuracy in grading for ethnical variations of the nasal valve angle. But since the dynamic physiology of the nasal valve is of major importance, camera-assisted analysis has to be video-based.

Materials and Methods

2.1 Materials

For the comparison, 4 types of sensors were ultimately selected. These included strain gauges, inductive sensors, optical sensors and video-assisted analysis. All were tested together and in relation to rhinomanometry which was performed with the 4-Phase Rhinomanometer, serial number 4-00178, by Rhinolab GmbH and its output was recorded using RhinoDMS altered LabView Edition and RhinoLab Doctor's edition 6.1.1.1503 by Rhinolab GmbH

During the development of all devices, standard crafting instruments were used. These comprised a multifunctional drilling and grinding tool, Dremel Model 800 Cordless Rotary Tool 10.8V, with various insertable heads. A soldering machine, JBC CD-2BE 140/75W by Welectron, together with soldering wire by FixPoint with a diameter of 0.56 mm and a ratio of 60% tin, 38% lead and 2% copper. A 2-K-epoxy glue, Uhu Plus Sofortfest 15ml by Uhu, was used for minor adhesive fixation.

3D-printing was performed with the 3D-printer Ultimaker 2 by Ultimaker with the Pro extension with PLA and ABS filaments of 2.85 mm diameter in various colors from Innofil 3D. The 3D-printer was controlled via the 3D-printing software Ultimaker Cura version 3.6, by Ultimaker.

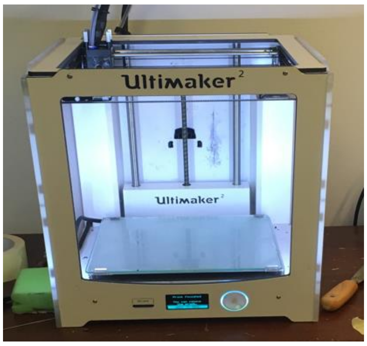

Figure 2.1 - 3D-printer Ultimaker 2

The strain gauge sensor was 1-LE11-3/350VE, produced by HBM. It features 350 ± 0.5 Ω (Ohm) resistance, 15.0 mm overall length, 3.0 mm grid length, 2.0 mm grid width.

Initially, two different inductive sensors were tested. These were the cylindrical sensor by Baumer, part number IR06.D03S-Q22.UA1Z.7SCV, and the rectangular sensor model DW-AS-509-C8-390 by Contrinex. The latter was then further implemented into data recording.

At the beginning, two different optical sensors were selected. The first was model GP2Y0A41SK0F distance measuring sensor by Sharp. The second was ILD1420-25CL1 optical sensor, by Micro-Epsilon. The wave length used by the laser is 670 nm, visible as red light and having a laser safety class level 1, giving it a very-low risk profile. The manufacturer provided a software, ILD1420 Tool V3.5.2, for data collection of this sensor. Again, only the latter was taken into field testing.

Video-assisted analysis was done by using a NanEye 2D image sensor and NanoUSB2 Eval Kit by AMS. The data was collected with the Awaiba Viewer V.2.23.3.2 software by Awaiba.

In order to calibrate the sensors prior to use, a set of gauge blocks with working standard units of up to 1.001 mm, HOLEX Endmaß-Satz Gen. 1 Art. No. 48045032 by Hoffmann Group, was used.

The mask that was modified and used for the comparison of the optical laser by MicroEpsilon and the strain gauge by HBM was produced by Dräger, Vollmaske Panorama Nova Model R26470. Several visors were used. For the manipulations of the visor, Paladur denture resin by Kulzer employed. The point of entry of the ILD1420-25CL1 optical sensor, laser class I by Micro-Epsilon, through the visor of the mask was secured by flange bearings and a central spherical ball by IGUS, part number EFOM-08.

The output of the inductive sensors and optical sensors was connected to an electrical 8-channel amplifier, GSV-8DS by ME-Meßsysteme. The recorded data was analyzed with the help of the GSVmulti software, version 1.42.

The calibration of the inductive sensor by Baumer was done using the oscilloscope by Meilhaus Electronics, MEphisto Scope UM202/UM203 and its software, MEphistoLab2, version 2.05.024.

Non-brand shrinkable tubing was also used to isolate wires and soldered connections. An industrial heater, model HL 2010 E by Steinel, was used to shrink these tubes and to shape the thermo splints that were initially used to create individual bite plates. The round thermo splints were manufactured by Henry Schein, part number 9001752. The size was 120 mm in diameter and 0.75 mm thick. The modulation of the splints was done by using Molding Plaster 5 kg by Krone with a density of 2,62 g/cm^3.

The safety and functionality of the electrical circuits was tested by using the digital multimeter, model DM830B by JPR Electronics. Furthermore, basic non-brand crafting parts such as screws, nuts, bolds, electrical cables and others were needed for the completion of each apparatus.

Equations that were presented in the “Literature Review” section were made using Daum Equation Editor, version 1.1.2 by Daum Communications.

Measurements from the use of strain gauges were recorded with RhinoDMS source version 14.0, a modified LabVIEW software. All data was stored as .xlsx-files via Microsoft Excel, version 16.22.

Selection of participants

The 10 participants that were selected were above the age of 18, did not have a medical history of nasal and/or upper airway pathology and did not suffer from an acute nasal and/or upper respiratory tract infection within the past two weeks prior to data collection. Furthermore, each volunteer must have been fully informed and have agreed to all aspects of the study process before enrolling in the program.

2.2 Methods

The development and construction of all devices was done at the MedTecResearch laboratory at Schwarzer Weg 3 B, 18292, Krakow am See, Alt-Sammit, Germany which belongs to the Center of Experimental Surgery of the University of Latvia, Faculty of Medicine.

2.2.1 Sensor Development

The strain gauge sensors were attached to a strip that was then placed into a 3D-printed U-shaped retainer to make each end of the strip bend towards the side of the nares. The retainer was then mounted onto a construction that was attached to a 3D-printed bite plate. All major parts were 3D-printed in series and secured with screws and other elements that make it easy to exchange the supporting bite plate before each measurement. The strain gauges are then connected via a flat cable that is lead outside of the mask across the rim to the rhinomanometer. The software RhinoDMS can then record nasal flow, pressure and, additionally, the data of the strain gauge.

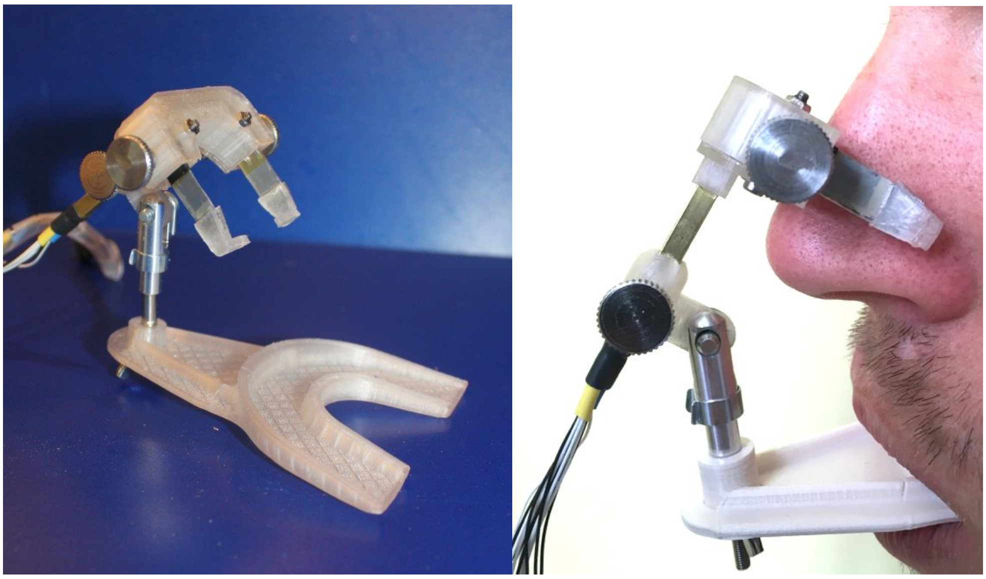

Figure 2.2 – Left: Strain gauge apparatus with 3D-printed bite plate, U-shaped sensor retainer and sensor heads; right: setup during clinical testing with the strain gauge sensing at the lateral external nasal wall

For the two sets of inductive sensors, a small piece of steel strip (see left on figure 2.3) was attached to the external location of the nasal valve on each side. The cylindrical inductive sensor, 6 mm in diameter and 22 mm in length with a measuring range from 0 to 3mm by Baumer, was held in position, closely lateral to the round piece of steel strip, by a headband construction. At this stage of development, only one unilateral sensor was employed. The electrical signal output was set to be 10 Volts at maximum.

Figure 2.3 - Left: Lateral view of the metal plate taped to the external nose; Right: Frontal view of the inductive sensor by Baumer in its retainer, positioned closely to the metal plate

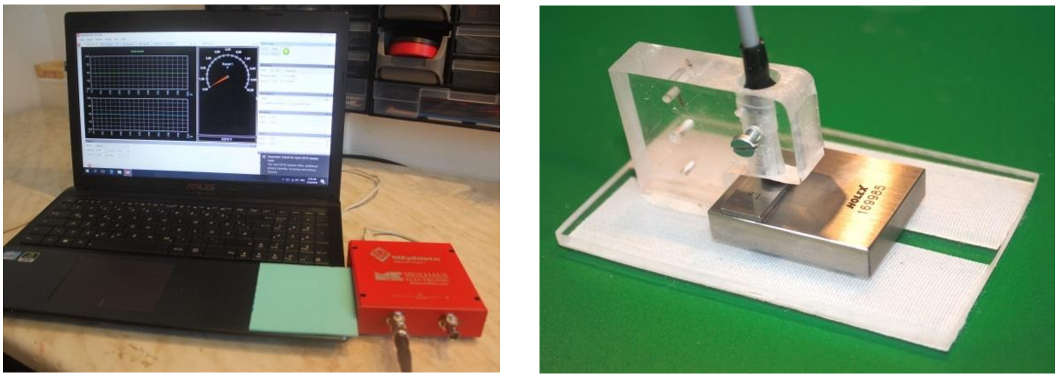

Figure 2.4 - Left: Calibration setup used for the inductive sensor by Baumer; Right: Apparatus holding the inductive sensor by Baumer in place

After the development of the measurement technique with this sensor, its calibration was performed. The oscilloscope recorded a systematic change of values for various distances between the sensor head and the metal object, realized with gauge blocks of the standard gauge set. 0mm represented a full distance of 3 mm, while at 2.8 mm only 0.2 mm distance between the sensor head and the metal plate remained. Each distance was measured three times in one round, with three rounds in total.

Due to the configuration and technical data, a second set of inductive sensors was added. These sensors by Contrinex were rectangular with 8mm width, 8mm height and 50mm length. As for the inductive sensor by Baumer, the electrical output was set to 10 Volts. The expected measuring range was 0 to 4 mm.

Figure 2.5 - Inductive sensors by Contrinex; blue circles mark the sensing area

The area of sensing, which is visible in figure 2.3 above, is located laterally at the tip of the device, allowing for the sensor to be placed closely to both sides of the external nose without needing a lot of the scarce space underneath the mask. The sensors were attached to a metal construction, giving them an upside-down V-shaped position that fit above the nasal ridge. A replaceable 3D-printed bite plate provided the necessary mounting support.

The sensors were connected to the 8-channel data amplifier via a cable that was placed through the front visor of the mask and soldered in to a plug fitting the analogue input of the amplifier. At the point of exit, the visor was modified with a 3D-printed element that was made air-tight with a rubber lining.

For practical purposes, the inductive sensors by Contrinex were dismounted and attached to a construction that enabled proper calibration. The standard gauges were then stacked up below both sensors. The height at which the sensors were positioned was 12.7 mm. The earliest possible results were expected at a stack of gauges equal or greater than 8.7mm, thus entering the range of these sensors from 0 to 4mm. The calibration was performed in three consecutive rounds obtaining three values for each distance.

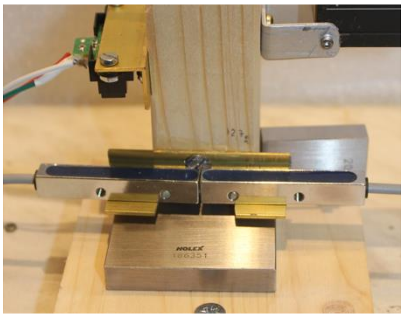

Figure 2.6 - Inductive sensors by Contrinex during calibration

The mounting support was initially planned to be provided by a headband as it was in use with the inductive sensor by Baumer, but then changed to a bite plate. Prior to involving 3D-printing, molding plaster was used to obtain a dental replica which was used to shape a temperature-sensitive splint into a bite plate by employing the industrial heater.

Figure 2.7 – Setup of the inductive sensor by Contrinex used in advanced laboratory testing showing the chrome-colored sensor with the blue sensing area on a 3D-printed mounting apparatus and bite plate

The two optical sensors that were selected for the project were firstly compared in the calibration stage, since a substantial difference in quality was already expected. The model by Sharp had a measuring distance of 4 to 30 cm and a voltage output of 0 to 5 V. The optical sensor by Micro-Epsilon had a precise measuring range starting at 25 mm distance from the object to 50 mm.

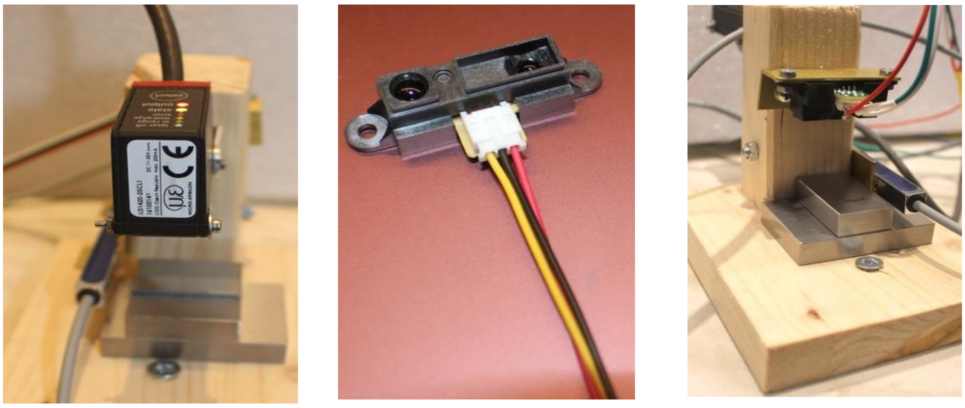

Figure 2.8 - Left: Optical sensor by Micro-Epsilon during calibration; Middle: Optical sensor by Sharp; Right: Optical sensor by Sharp during calibration

After the first calibration round of the Sharp sensor, obtaining one value for each distance, it was excluded from the project due to its results. As seen in figure 2.8 above on the left, the Micro-Epsilon sensor was then mounted at the height of 59 mm above ground and standard gauges were placed below it in three consecutive sessions, registering one measured value per distance at a calculated scale of 0.13588 from volt to millimeter.

Then the sensor by Micro-Epsilon was fixed at the end of a hollow, approximately 10cm long metal tube through which the wire of the sensor was guided. The sensor was placed within the mask laterally in a custom-built box within the visor and the metal tube containing the wire passed outward through the box with the help of an air-tight bearing with a central spherical element through which the metal tube was directed. This allowed external control of the position of the laser under full visibility without compromising the mask. The laser could now be adjusted to record movement of the right lateral nasal wall and also to verify the results of the strain gauge by measuring its displacement directly.

Figure 2.9 – View of the interior of the facemask used in participant-testing with the optical sensor by MicroEpsilon below the visor on the right

The nano-camera was fixated to a metal pin and placed within the nasal vestibule in order to give full visibility of the nasal valve internally. After positioning the camera, a video was recorded for 15 to 30 seconds during normal nasal breathing.

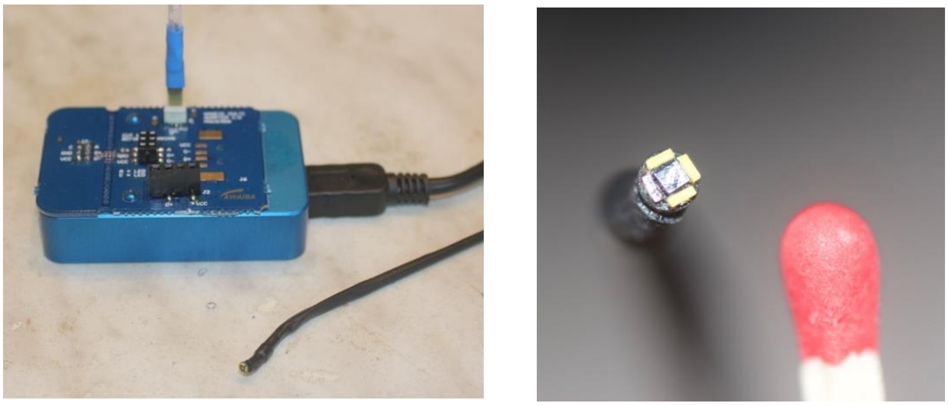

Figure 2.10 - Left: Blue camera terminal with the camera pin in the front; Right: Camera size compared to a match head

Figure 2.11 – Image showing the setup for comparison used in participant testing with the strain gauge placed on the lateral external nasal wall, the laser directed at it on the right side of the nose and the 4-phase rhinomanometer recording

2.2.2 Measurements

All electrical sensors had to pass through the safety and the calibration stage before participant testing.

The video-assisted analysis was performed without using the mask for rhinomanometry. The camera was inserted into the vestibule and a video was recorded during nasal breathing. In theory, the footage could then be analyzed by measuring the change of the black surface area representing the patent airway at the level of the nasal valve.

Generally, the main measurement process was coordinated in two stages. Firstly, the participant underwent standard rhinomanometry, bilaterally and without any additional sensors, to record the prevalent nasal physio-anatomy. In the second stage, the strain gauges together with the laser sensor from MicroEpsilon were adjusted to record at the level of the nasal valve on the lateral part of the external nose. The patient was then asked to breathe three times in and out calmly, three times as deeply and then to exhale three times as strongly as possible. These actions were simultaneously recorded by the rhinomanometer which was attached to the mask and the strain gauges together with the laser sensor to obtain directly comparable set of data to validate the functionality, accuracy and practicability of the strain gauges versus the laser sensor.

With the MicroEpsilon optical sensor, we also obtained data samples in laboratory testing of calm, regular nasal breathing that shows the nasal valve motility.

Figure 2.12 – 4-phase rhinomanometer used during participant testing

2.2.2 Data analysis

The analysis and graphic presentation of the laboratory-stage calibration was done via Microsoft Excel, version 16.22. The sensor calibration was realized by scaling the sensor output in volts to millimeter using the standard gauges. The scaling factor was then used to transform the data collected from the participants.

The rhinomanometry data was saved as PDF-files and analyzed for right nasal obstruction using the LogReff value and the clinical rhinomanometry classification by Vogt et. al (Vogt et al. 2016).

The participant data of the second stage of measurements was stored as CSV-files, and TXT-files from RhinoDMS. The two file types were then combined using an executive program created by Matthias Prill in order to receive and identical time stamp for both, the MicroEpsilon sensor and the strain gauges. With the help of the calculated scaling factors, we obtained measurements in millimeter that were compared in order to investigate the accuracy of the strain gauge measurement in a clinical setting. All data graphs shown in the "Results" section were made with Microsoft Excel, version 16.22.

2.2.3 Ethical considerations

This study received the approval of the Institute of Scientific Research Ethics of the Institute of Cardiology and Regenerative Medicine of the University of Latvia. All actions were performed under ethical consideration and designed to fulfil all modern standards of proper, open and participant-centered conduct.

All participants received a thorough introduction and explanation of the study program and its purpose in oral as well as in written form. It was encouraged to ask any questions that arose, and participants were reassured that declining the offer prior and also after initially agreeing to the participation was possible and uncomplicated.

Participants were asked to sign a written informed consent. The collection of signed consent forms was stored safely at the Center of Experimental Surgery in a lockable drawer.

Results

3.1 Laboratory-based testing

Optical analysis by the Nano-camera

It was possible to obtain high-resolution video footage at the level of the nasal valve during deep nasal breathing. The video data gave visual insights into the dynamic of the lateral nasal wall. Regarding the quantification of such data, it became apparent that the repeatability of this technique, within the limits of our setup, was underwhelming and highly dependent on the angle, position and lighting during each session. The figures below show a repeated measurement of the same valve region of the same nose with seemingly improved visibility. Under these circumstances we cannot make conclusive statements about the nasal valve from our footage collected based on the dynamic changes seen between in- and expiration.

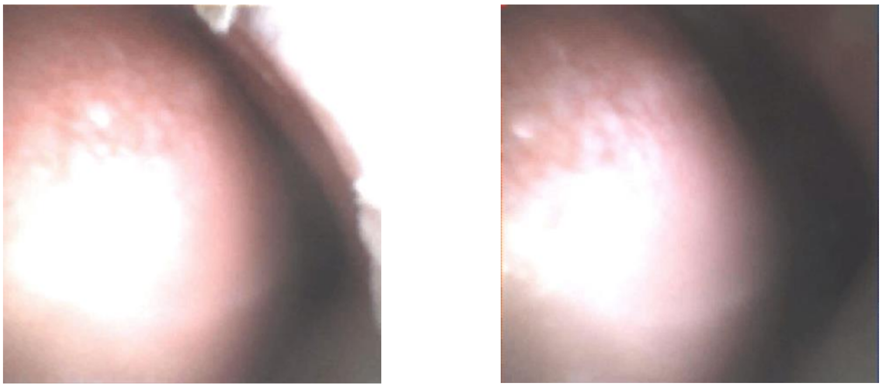

Figure 3.1 – Nano-camera image of the left nasal vestibule, septum on the left, lateral wall on the right; left: during peak inspiration; right: During peak expiration

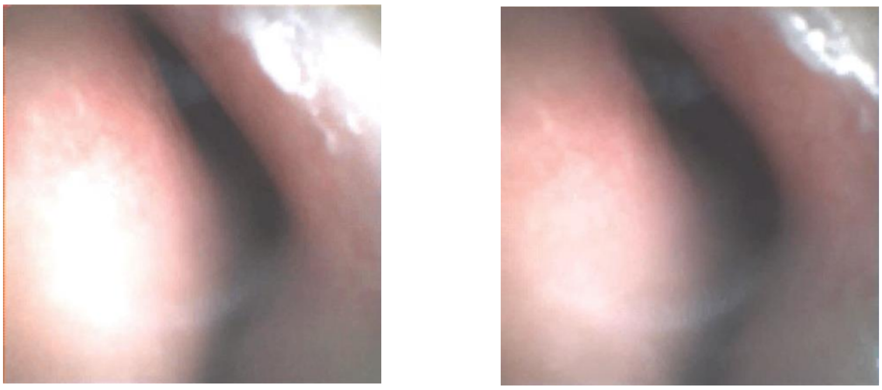

Figure 3.2 – Repeated second time imaging of the left nasal vestibule, septum on the left, lateral wall on the right; left: during peak inspiration; right: during peak expiration

Inductive Sensors

The calibration of the Contrinex inductive sensor showed an accuracy that is highest at mid-range distance to the target object and falls at ranges closer than 1.1 mm sharply. Above that cut-off, the accuracy averages at 96,53% (see figure 3.3).

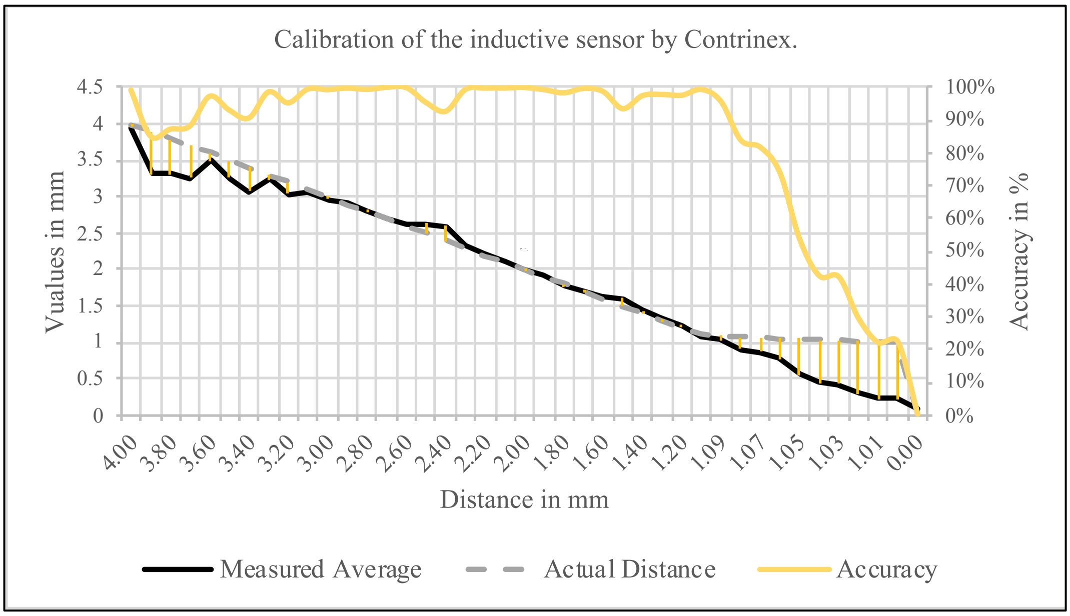

Figure 3.3 - Calibration chart of the inductive sensor by Contrinex with the measured average in mm (black line), actual distance in mm (dashed grey line) and the sensor's accuracy in % (yellow line)

Optical Sensors

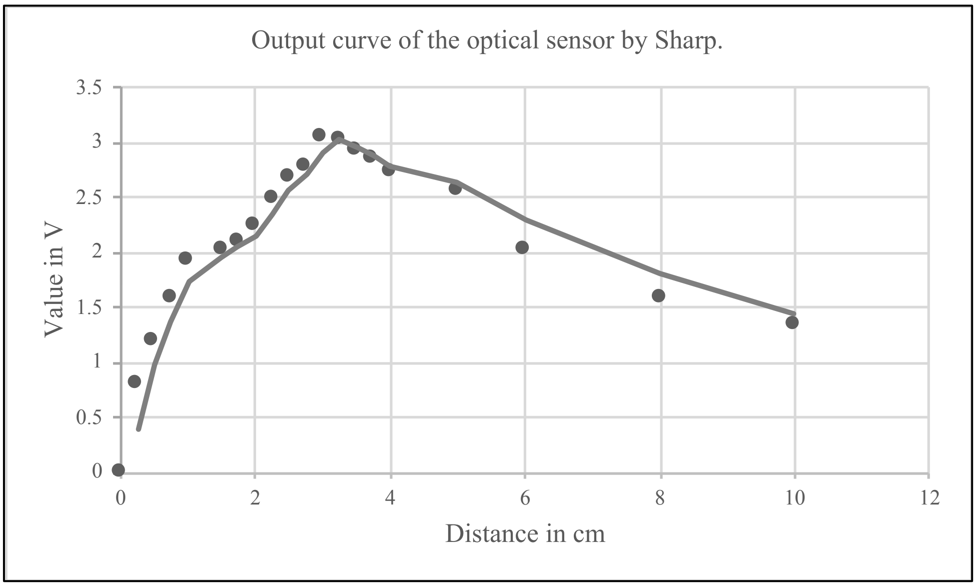

Figure 3.4 - Output graph of the optical sensor by Sharp with trendline showing the moving average

The basis of using infrared light such as in the sensor by Sharp, emerged as an unsuitable technique for our purposes due to its alteration in measurements depending on the light reflected by the object and the invisibility of its focusing point. Both of these disadvantages were not present in the laser-based optical sensors by MicroEpsilon. The sensor by MicroEpsilon showed high accuracy throughout the measurement range during calibration with an overall average of 99.63% accuracy (see figure 3.5).

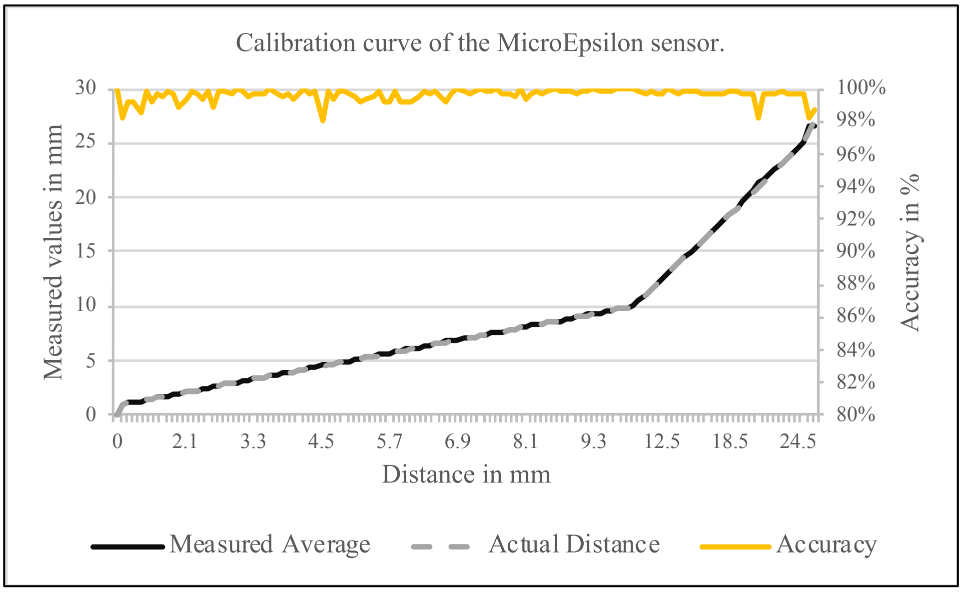

Figure 3.5 – Calibration curve of the optical sensor by MicroEpsilon; It shows the measured average in mm (black line), the actual distance in mm (dashed grey line) and the measurement accuracy in % (yellow line)

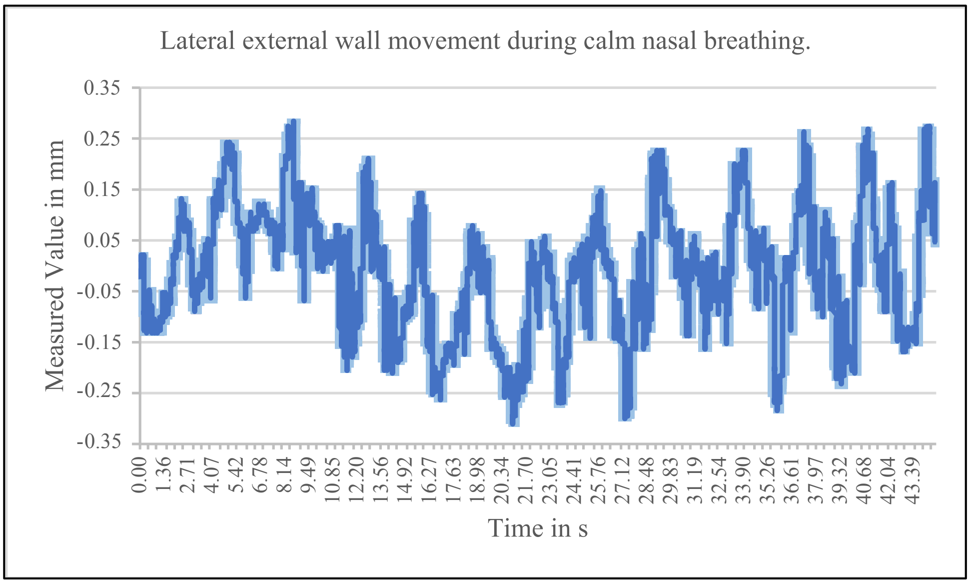

Figure 3.6 – Lateral external wall movement measured by the MicroEpsilon optical sensor at a distance of 19.35mm at 2000 Hz (dark blue line); the error of measurement of 0.37% is marked as a light blue halo

During calibration, the strain gauge sensors proved to have an average accuracy of 96.20% with a decline for measurements past 3 mm of displacement (see figure 3.7).

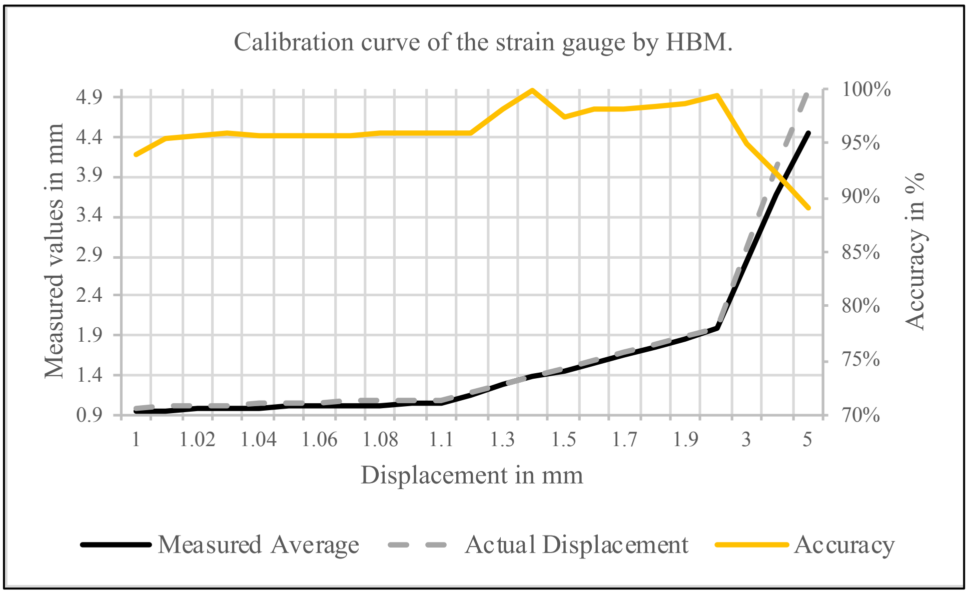

Figure 3.7 – Calibration curve of the strain gauge by HBM; It shows the measured average in mm (black line), the actual displacement in mm (dashed grey line) and the accuracy of strain gauges in % (yellow line)

3.2 Participant-based testing

We recorded the preemptive rhinomanometry analysis for all participants and were able to obtain substantial data in the comparison of the optical sensor by MicroEpsilon versus the strain gauge by HBM for all but one participant.

Out of the 10 volunteers there were (n=4; 40.0%) male and (n=6; 60.0%) female with a mean age of 32.9 (±11.51) years. Prior rhinomanometry showed an average logReff for the right nasal cavity of 0.478 ((±0.43) without decongestion. 6 values were class I (<0.70), 2 values class II (0.7-0.9), 1 value class III (0.9-1.1) and 1 value class IV (1.1-1.4) (see classification table on page 22). Within the study group, the mean air flow was 531.20 sccm/s (± 38.41) and the mean pressure 164.54 Pa (±51.09).

With the measurement obtained with the optical sensor by MicroEpsilon which are shown in figure 3.8, we confirmed that the movement of the lateral external nasal wall begins instantly at the onset of nasal breathing.

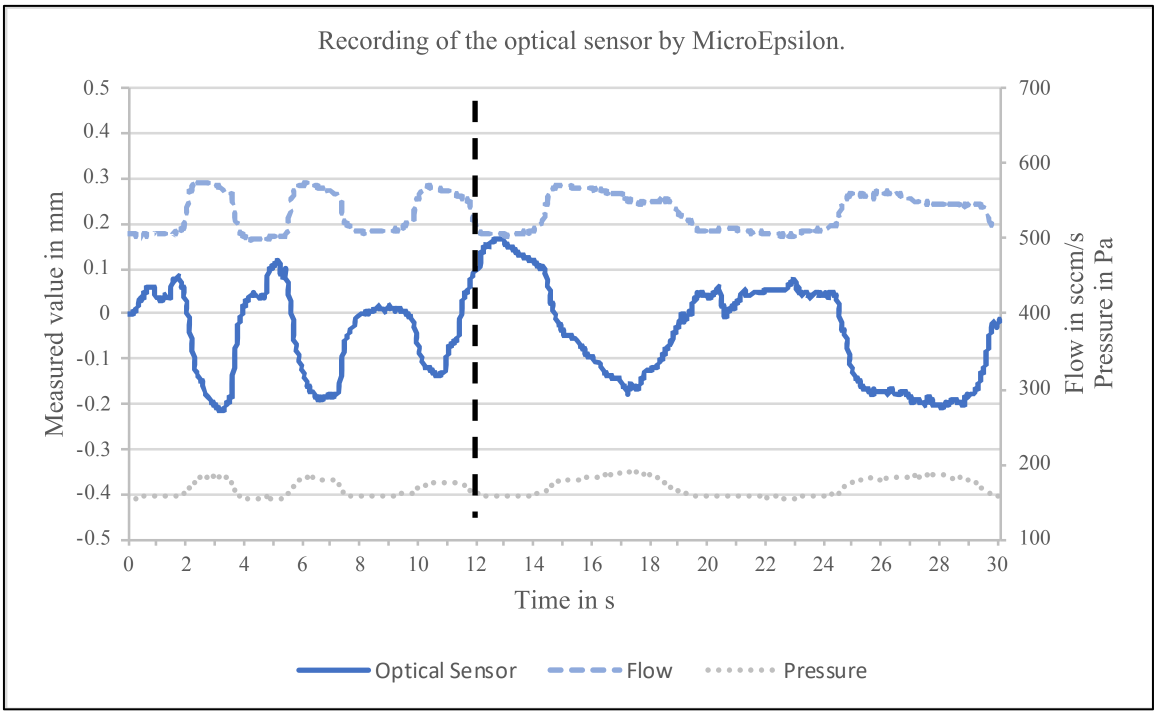

Figure 3.8 – Graph showing two-stage nasal breathing measured with the optical sensor by MicroEpsilon, in reference to flow in sccm/s (dashed light blue line) and pressure in Pa (dotted grey line) measured by the rhinomanometer; the dashed black line is separating the first three normal nasal breathing cycles and the two forced deep nasal breathing cycles

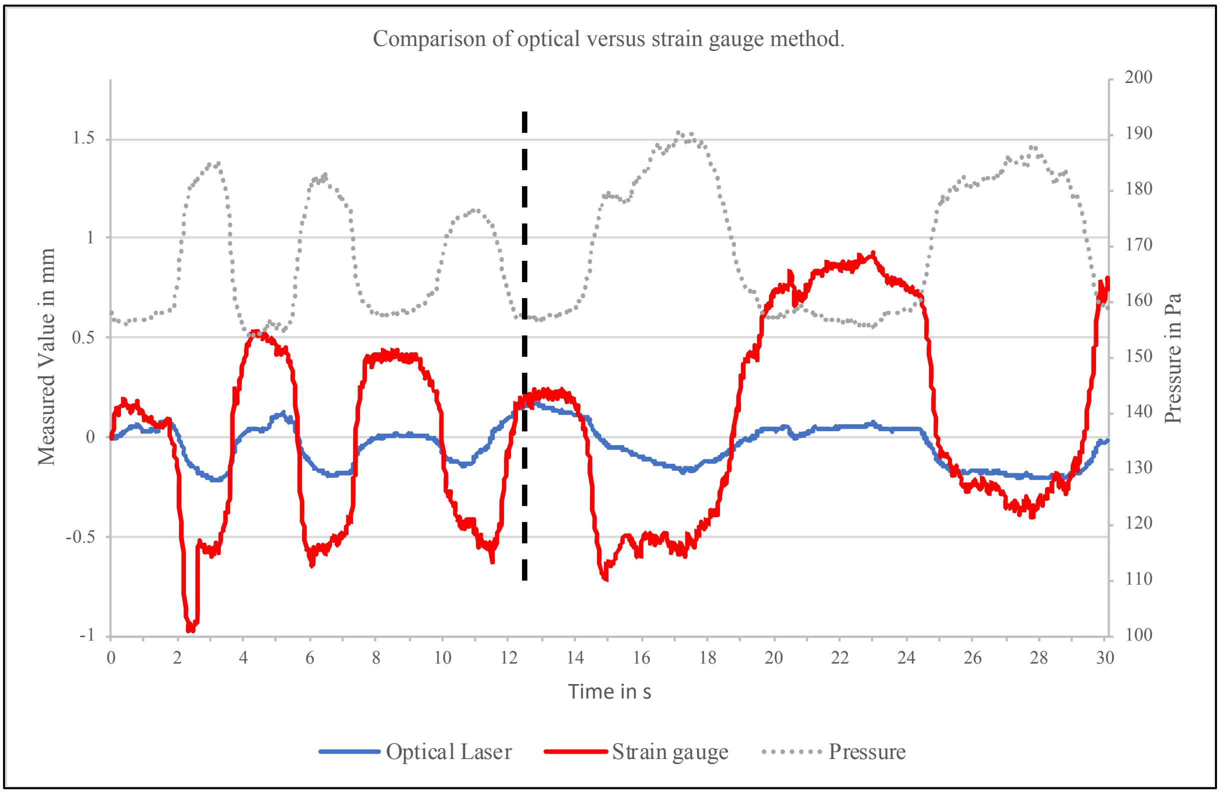

Figure 3.9 – Graph showing experimental simultaneous measurements in mm with the optical sensor by MicroEpsilon (blue line) and the strain gauge by HBM (red line) in respect to pressure in mbar (grey line) recorded by the rhinomanometer

Discussion

It is paramount to establish a reliable diagnostic assessment of the nasal valve. However, its anatomical and physiological characteristics make it difficult to develop a reliable diagnostic device. In theory, such intended analysis must investigate first the breathing-dependent displacement of the lateral external nasal wall and second the mechanical properties of the anatomical structures, such as rigidity. Within the framework of this diploma thesis, it was necessary to investigate, in the first instance if the displacement of the valve as observed last year by Akmenkalne and Vogt (Akmenkalne et al. 2018) using strain gauge technology can be confirmed by other, technically entirely different, methods. Therefore, we commenced to develop and adapt techniques for distance measuring, including such that are widely used in other fields of science for this particular task. The testing had to be performed according to the criteria of feasibility, economic aspects and medico-technical safety.

For sensors that were taken from laboratory-testing into participant-testing, we experienced in almost all cases difficulties in obtaining valid elastographic data. The stability of the sensor in a clinical setting was a key issue due to the extremely early onset of nasal movement and any instability came at the cost of loss of accuracy of the measurement. The 3D-printed bite plates gave an immediate improvement in stability compared to the customized thermo splints we used initially. Another factor was the transmission of the measured data from the sensors to the recorder through the facemask via cables as they would often compromise the position of the sensors during the setup of the measurements. We also encountered difficulties in positioning the sensors towards the same measuring point on the lateral external nasal wall. We found such techniques advantageous where the focusing point of the sensor was clearly visualized.

We implemented a setup for camera-assisted analysis to compare it to the publication of Patel et al. (2018) which used a subjective visual grading scale for the evaluation of the nasal valve. From that we concluded that firstly, the camera-assisted analysis would have to be dynamic, thus video-based, in order to observe the motion and secondly, objectified. In order to objectify the assessment, it was theorized to record the change of the size of the black surface representing the nasal lumen at the level of the nasal valve by optical processing. However, it became apparent that the camera analysis is hardly reproduceable in our setup and thus did not allow further processing.

Inductive sensing was the next technique that was tested during our project. After changing the shape and technical configuration of the sensor by Baumer to the one by Contrinex, we took the latter into advanced laboratory testing. It showed that due to the nature of inductive sensing, it presented itself impossible to place the inductive sensor in a distance of 4mm to the lateral nose and keeping it stable while the participant advanced her/his head into the facemask. Two major hurdles were seen in the limited space of the facemask and the stability of the sensor apparatus.

Two types of optical sensors were selected. The use of the sensor by Sharp was ruled out during the calibration stage due to two major disadvantages. The first being its sensitivity to the target object's color; the second was its inverted calibration curve for a distance of approximately 3cm and closer (see figure 3.4). During the construction of the head apparatus with the rhinomanometry facemask, it showed that the range around 2.5 to 5 cm would be a crucial part of the measuring range and therefore would pose major difficulties due to is non-linear scaling. High-quality optical sensors such as those by MicroEpsilon are a core measurement modality that is able to provide exact distance measurements and references versus other sensor types. However, since the quality of this sensor type varies greatly with the price, the use of optical sensors requires a greater financial freedom. Optical sensing has the advantage of having a higher longevity and better hygienic profile in the clinical setting. Thus, it was selected to verify and compare to the performance of the strain gauge in a clinical setting

The initial consideration for the participant stage of sensor testing was, due to our experience with the optical sensor by MicroEpsilon, to verify the strain gauge measuring technique by focusing the optical sensor on the outer surface of the strain gauge at the level of the nasal valve and thus being able to make a conclusion about the accuracy of the latter. In spite of that, an accurate verification in respect to the accuracy of obtained data by the strain gauge was not possible within the setup. The two sensors showed a relevant nonconformity throughout the study population with a large difference in quality. The difference shows that the strain gauge technique has yet to be improved in order to be suitable for quantitative elastography in respect to the early onset of motion of the nasal valve.

At the end of the technical analyses, it could be stated that many methods for distance measuring deliver exact and reproducible results in the range of the expected movement of the nasal valve. High-resolution nano-cameras, as we used in the study, are currently priced at more than 300 Euro and are exposed to a strong degree of wear when being used in the humid environment of the nasal vestibule. Inductive sensors are available at ranges starting from 50 € and more depending on the quality chosen. Optical sensors currently have a wide range of prices, from 10 € (sensor by Sharp) to more than 1000 € for laser-based sensors such as the one by MicroEpsilon. The prices for strain gauges start from as low as 4 € per gauge and could therefore be considered for a single-use medical product.

In conclusion, strain gauges can be adapted with the highest probability to a diagnostic measurement technique with a bearable economic impact.

Table 3.1	*Accuracy*	*Reproducibility*	*Economic Impact*	*Comments*
Camera analysis		Limited	High	Qualitative only
Inductive sensing	High	Limited	Moderate	
Optical sensing	Very High	High	High	Essential reference tool
Strain gauge	High	Moderate (currently)	Low	

Table 3.1 – Summary of each sensing modality and its evaluation according to the pilot study's observations

It should be emphasized that the small set of tests on participants confirm that the movement of the lateral nasal wall already starts in very low pressure or flow rates. Thus, the proposition of the study could be confirmed validated.

Conclusions

By different technical methods, it is possible to determine the breathing-dependent movement of the lateral external nasal wall and thus, characterizing the nasal valve. The results of elastography of the nasal valve show close relations to the loops in 4-phase-rhinomanometry. Initial tests performed by such methods confirm that the elasticity of the nose has to be conjointly considered in the context of indications of rhinoplastic procedures as a dynamic component in Computational Fluid Dynamics.

Camera-assisted analysis does not yet provide objective quantifiable measurements of the motility of the nasal valve but may have a promising future in regard to dynamic analysis.

Optical sensing showed to be a powerful and accurate way to observe and quantify nasal valve movement. It also helps to verify other modalities. These methods follow various principles, whereas laser-based measurements seem to deliver the most precise results.

A technically feasible method for measuring the nasal elasticity has to be developed as well as a method for the analysis of the physical properties. Presently, modifications of strain gauge technique seem to fulfill the most requirements.

Bibliography

Akmenkalne, L., Vogt, K., Peksis, K., (2018), Quantitative Determination of the Motility of the Nasal Valve, Diploma Thesis, University of Latvia

Chandra, R. K., Patadia, M. O., Raviv, J., (2009), Diagnosis of Nasal Airway Obstruction, The Otolaryngologic Clinics of North America, 2009-04-01, Volume 42, Issue 2, Pages 207-225

Clement, P., Halewyck, S., Gordts, F., Michel, O., (2014) Critical evaluation of different objective techniques of nasal airway assessment: a clinical review. Eur Arch Otorhinolaryngol. 2014 Oct;271(10):2617-25.

Cottle, M., (1968), Rhino-sphygmo-manometry: an aid in physical diagnosis. Int Rhinol 1968; 6(1/2):7–26

Courtade, A., (1903), Étude clinique et physiologique de l'obstruction nasale, Arch. Internat. Laryng.

Dhingra, P.L., Dhingra, S., Dhingra, D., (2014) Disease of Ear, Nose and Throat & Head and Neck Surgery, 6th Edition, Section II, p. 133-178

Dinardi, R., De Andrade, C., Da Cunha Ibiapina, C., (2017), Effect of the external nasal dilator on adolescent athleteswith and without allergic rhinitis, International Journal of Pediatric Otorhinolaryngology, 2017-06-01, Volume 97, Pages 127-134

Dinardi, R., De Andrade, C., Martins-Costa, H., Da Cunha Ibiapina, C., (2016), Does the Airmax internal nasal dilator increase peak nasal inspiratory flow (PNIF) in adolescent athletes?, International Journal of Pediatric Otorhinolaryngology, 2016-05-01, Volume 84, Pages 37-42

Doyle, J., O'Grady, K., (2018) Physics of the Airway in Hagberg and Benumof's Airway Management 2nd Edition by Hagberg, C. A., Artime, C. A., Aziz, M. F., Chapter 4, p. 92-109

Drake, R. L., Vogl, A. W., Mitchell, A. W., (2018) Gray's Basic Anatomy, Second Edition, Chapter 8, p. 413-596

Eccles, R., (2014) The nose and control of nasal airflow in Middleton's Allergy: Principles and Practice by Adkinson, N. F., Bochner, B. S., Burks, A. W., Busse, W. W. Holgate, S. T., Lemanske, R. F., O'Hehir, R. E., 8th Edition, Chapter 40, p. 640-651

Guyuron, B., (2012) Rhinoplasty, Chapter 1, p.1-26

Harten, U., (2011) Physik für Mediziner Springer Verlag 13th Edition, Chapter 3, p. 88-98

Hoffmann, K. (1987). Eine Einführung in die Technik des Messens mit Dehnungsmessstreifen. Hottinger Baldwin Messtechnik GmbH

Jian, H. Z., Heow, P. L., Kian, M. L., Shu, J. L., De, Y. W., (2011) Evaluation and comparison of nasal airway flow patterns among three subjects from Caucasian, Chinese and Indian ethnic groups using computational fluid dynamics simulation, Respiratory Physiology & Neurobiology,, Volume 175, Issue 1, Pages 62-69, Copyright © 2010 Elsevier B.V.

Jones, N., (2001) The nose and paranasal sinuses physiology and anatomy. Advanced Drug Delivery Reviews. https://doi.org/10.1016/S0169-409X(01)00172-7)

Knowlton, F. P., Starling, E. H. (1912). The influence of variations in temperature and blood-pressure on the performance of the isolated mammalian heart. The Journal of Physiology, 44(3), 206–219.

Lund, V. J., Stammberger, H., Fokkens, W. J., (2014) European Position Paper on the Anatomical Terminology of the Internal Nose and Paranasal Sinuses, Rhinology Journal, Supplement 24, p. 4-17

Malaty, J., (2018) Facial and Skull Fractures in *Fracture Management for Primary Care Updated Edition* by Eiff, M., Hatch, R., 3rd Edition, Facial and Skull Fractures, Chapter 17, p. 327-340

Marin,V. P., Cochran,C. S., Gunter,J. P., (2009) Anatomic approach for tip problems. In: Aston SJ, et al, editors. Aesthetic plastic surgery. St Louis (MO): Elsevier. p. 507–521

Masing, H., (1965), Die klinische Bedeutung der Nasenwiderstandsmessung. Eur Arch Otorhinolaryngol 1965; 185(2):763–767

Miyahara, Y., Ukai, K., Yamagiwa, M., Ohkawa, C., Sakakura, Y., (1998), Nasal passage patency in patients with allergic rhinitis measured by acoustic rhinometry: nasal responses after allergen and histamine provocation, Auris Nasus Larynx, Volume 25, Issue 3, Pages 261-267

Neligan, P., Buck, D., (2014), Chapter Rhinoplasty, Core Procedures in Plastic Surgery, Chapter 3, Pages 46-70

Nigro, C. E. N., Nigro, J. F. D. A., Mion, O., & Mello, J. F. (2009). Nasal Valve: Anatomy and physiology. Brazilian Journal of Otorhinolaryngology. https://doi.org/10.1016/S1808-8694(15)30795-3

Pallanch, J., Jorissen, M., (2015), Objective Assessment of Nasal Function, Cummings =Otolaryngology, 40, 644-657.e4

Patel, B., Virk, J. S., Randhawa, P. S., & Andrews, P. J. (2018). The internal nasal valve: a validated grading system and operative guide. European Archives of Oto-Rhino-Laryngology, 275(11), 2739–2744. https://doi.org/10.1007/s00405-018-5142-x

Pirila, T., Tikanto, J., (2009) Acoustic rhinometry and rhinomanometry in the preoperative screening of septal surgery patients. Am J Rhinol Allerg 2009; 23(6):605–609

Probst, R., Grevers, G., Iro, H., (2017) Basic Otorhinolaryngology - 2nd Edition, Chapter 1, p. 2-13

Rohrich, R. J., (2018) Nasal Analysis and Anatomy in *Plastic Surgery: Volume 2: Aesthetic Surgery* by Rubin, J. P., Neligan, P. C., Chapter 15, 417-429

Samra, S., Steitz, J., Hajnas, N., Toriumi, D., (2018), Surgical Management of Nasal Valve Collapse, Otolaryngologic Clinics of North America, The, 2018-10-01, Volume 51, Issue 5, Pages 929-944

Seren, E., (2009) A New Surgical Method of Dynamic Nasal Valve Collapse. Arch Otolaryngol Head Neck Surg. 2009;135(10):1010–1014. doi:10.1001/archoto.2009.135

Som, P. M., Lawson, W., Fatterpekar, G. M., Zinreich, S. J.,Shugar, J. (2011) Embryology, Anatomy, Physiology, and Imaging of the Sinonasal Cavities , Head and Neck Imaging, Chapter 2, 99-166

Sowder, J. C.,Thomas, A. J., Ward, P. D., (2017), Essential Anatomy and Evaluation for Functional 2017-05-01, Volume 25, Issue 2, Pages 141-160, Rhinoplasty Facial Plastic Surgery Clinics of North America

Stehning, C., (1999), Meßtechniken und Schaltungsentwürfe zur hochpräzisen Abstandsmessung mit Ultraschall, Projektarbeit, Elektrotechnik, Universität Bremen

Stevens, M. R., Emam, H. A., (2012) Applied Surgical Anatomy of the Nose, Oral and Maxillofacial Surgery Clinics, Volume 24, Issue 1

Tal, A., (2014) Obstructive Sleep Apnea Syndrome: Pathophysiology and Clinical Characteristics in Principles and Practice of Pediatric Sleep Medicine 2nd Edition by Sheldon, S. H., Ferber, R., Kryger, M. H., Gozal, D., Chapter 27, 215-220

Teixeira, R. U., Zappelini, C. E., Alves, F. S.,da Costa, E. A., (2011), Peak Nasal Inspiratory Flow Evaluation as an objective method of measuring nasal airflow, Brazilian Journal of Otorhinolaryngology. Volume 77, Issue 4. Pages 473-480

Uddströmer, M., (1940), Acta Otolaryngologiea Supplement 42 p. 69, 1940. Nederlands Tijdschrift voor Geneeskunde 25: 297

Vogt, K., Wernecke, K. D., Behrbohm, H., Gubisch, W., & Argale, M. (2016). Four-phase rhinomanometry: a multicentric retrospective analysis of 36,563 clinical measurements. European Archives of Oto-Rhino-Laryngology

Vogt, K. Bachmann-Harildstad, G., Lintermann A., Nechyporenko, A., Peters, F., Wernecke, K., (2018),The new agreement of the international RIGA consensus conference on nasal airway function tests, Rhinology 56: 0-0 2018, in press

Wang, D., (2014), Basics of Capacitive Sensing and Applications, Application Report, Texas Instruments

Acknowledgements

I first and foremost have to thank my supervisor Prof. Dr. Dr. Klaus Vogt for his help, his strive and his friendship. I am very grateful for being part of this project. I also thank Matthias Prill for his effort and help. He provided the necessary expertise in electronics and software.

I also have to thank Elīza Poikāne, Uta Vogt, Kaspars Peksis and many others for their support and input. Lastly, I express my gratitude to all participants for making this study possible.

DOCUMENTATION PAGE

This Diploma Thesis

„____

____

____”

was developed at the Faculty of Medicine of the University of Latvia.

With my signature, I attest, that this research has been carried out without aid or assistance. Used information was obtained only from indicated sources and the electronically submitted copy of this diploma work complies with printout.

Author: _________________________ _____________________

(name, surname) (*signature)*

I recommend the work for presentation.

Supervisor: ______________________ ______________________ _____________

(position, name, surname, degree) *(siganture)* *(date)*

Reviewer: ______________________ _______________________ ______________

(position, name, surname, degree) *(signature)* *(date)*

The diploma thesis was submitted to the Faculty of Medicine on: _______________

(date)

International students' coordinator, _____________________________________

(signature)

The diploma thesis is presented at the meeting of the State Examination Commission of Higher Professional Study Program „Medicine”___________2019. Protocol No. ______________

Secretary of Commission: __________________________ _____________________

(position, name, surname, degree) *(signature)*